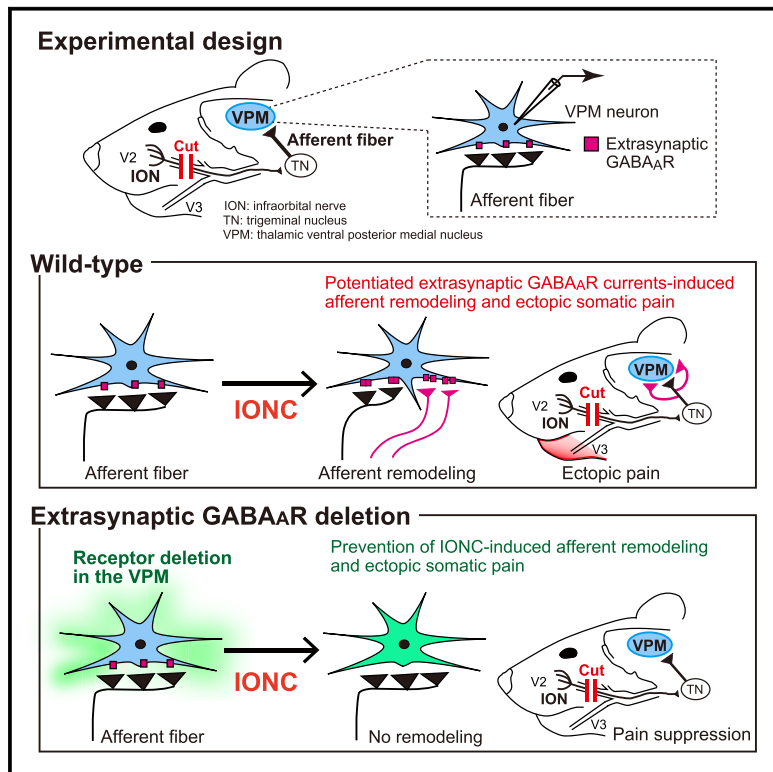


Tonic GABAergic Inhibition Is Essential for Nerve Injury-Induced Afferent Remodeling in the Somatosensory Thalamus and Ectopic Sensations

Graphical Abstract



Authors

Yasuyuki Nagumo, Yoshifumi Ueta,
Hisako Nakayama, ..., Naofumi Uesaka,
Masanobu Kano, Mariko Miyata

Correspondence

mmiyata@tamu.ac.jp

In Brief

Infraorbital nerve cut causes functional and structural remodeling of neural circuits in the somatosensory thalamus, forming the basis for somatotopic reorganization and ectopic sensations. Nagumo et al. report that injury-induced potentiation of extrasynaptic GABA_AR currents are a key player in induction and maintenance of the remodeling and ectopic somatic sensations.

Highlights

- Infraorbital nerve cut (IONC) causes thalamic afferent remodeling and ectopic pain
- IONC increases extrasynaptic GABA_ARs (eGABA_ARs) in remodeled thalamic neurons
- Thalamic eGABA_ARs are necessary for induction and maintenance of the remodeling
- Absence of eGABA_ARs in the thalamus prevents ectopic pain



Article

Tonic GABAergic Inhibition Is Essential for Nerve Injury-Induced Afferent Remodeling in the Somatosensory Thalamus and Ectopic Sensations

Yasuyuki Nagumo,^{1,2} Yoshifumi Ueta,^{1,6} Hisako Nakayama,^{1,6} Hironobu Osaki,¹ Yuichi Takeuchi,¹ Naofumi Uesaka,^{3,4} Masanobu Kano,^{3,5} and Mariko Miyata^{1,7,*}

¹Department of Physiology, Division of Neurophysiology, School of Medicine, Tokyo Women's Medical University, Tokyo 162-8666, Japan

²International Institute for Integrative Sleep Medicine (WPI-IIIS), University of Tsukuba, 1-1-1 Tennodai, Tsukuba, Ibaraki 305-8575, Japan

³Department of Neurophysiology, Graduate School of Medicine, The University of Tokyo, Tokyo 113-0033, Japan

⁴Department of Cognitive Neurobiology, Graduate School of Medical and Dental Sciences, Tokyo Medical and Dental University, Tokyo 113-8510, Japan

⁵International Research Center for Neurointelligence (WPI-IRCN), The University of Tokyo Institutes for Advanced Study (UTIAS), The University of Tokyo, Tokyo 113-0033, Japan

⁶These authors contributed equally

⁷Lead Contact

*Correspondence: mmiyata@tamu.ac.jp

<https://doi.org/10.1016/j.celrep.2020.107797>

SUMMARY

Peripheral nerve injury induces functional and structural remodeling of neural circuits along the somatosensory pathways, forming the basis for somatotopic reorganization and ectopic sensations, such as referred phantom pain. However, the mechanisms underlying that remodeling remain largely unknown. Whisker sensory nerve injury drives functional remodeling in the somatosensory thalamus: the number of afferent inputs to each thalamic neuron increases from one to many. Here, we report that extrasynaptic γ -aminobutyric acid-type A receptor (GABA_AR)-mediated tonic inhibition is necessary for that remodeling. Extrasynaptic GABA_AR currents were potentiated rapidly after nerve injury in advance of remodeling. Pharmacological activation of the thalamic extrasynaptic GABA_ARs in intact mice induced similar remodeling. Notably, conditional deletion of extrasynaptic GABA_ARs in the thalamus rescued both the injury-induced remodeling and the ectopic mechanical hypersensitivity. Together, our results reveal a molecular basis for injury-induced remodeling of neural circuits and may provide a new pharmacological target for referred phantom sensations after peripheral nerve injury.

INTRODUCTION

Peripheral nerve injury frequently triggers referred phantom sensations that are perceived at a location other than the injured site. Functional brain imaging and electrophysiological studies identified that peripheral nerve injury causes maladaptive plastic changes along the somatosensory pathways, including somatotopic reorganization; the degree of which is highly correlated with phantom pain and/or sensation (Eto et al., 2011; Graziano and Jones, 2009; Jones and Pons, 1998; Kim and Nabekura, 2011; Takeuchi et al., 2012; Wang and Thompson, 2008). Furthermore, synaptic connections in the central nervous system (CNS) are dynamically remodeled by peripheral nerve injury (Kim et al., 2016; Kim and Nabekura, 2011). We found that complete transection of the whisker sensory nerve induces functional remodeling of afferent fibers in the somatosensory thalamus, such that the number of afferent inputs onto each thalamic neuron increases from one to many (Takeuchi et al., 2012). This remodeling is closely associated with somatotopic reorganization and ectopic mechanical hypersensitivity in the mandibular region

(Takeuchi et al., 2017). However, although dynamic remodeling of CNS neuronal circuits by peripheral nerve injury has been intensively investigated, the underlying molecular mechanisms remain largely unknown.

γ -Aminobutyric acid (GABA)-mediated inhibition has been proposed to be crucial for the initiation and maintenance of somatotopic reorganization in the CNS induced by peripheral nerve injury. The protein and mRNA expression levels of the GABA_A receptors (GABA_ARs), glutamate decarboxylase (GAD), and GABA in the CNS are altered after nerve injury (Castro-Lopes et al., 1993; Fukuoka et al., 1998; Jones and Pons, 1998; Moore et al., 2002; Mowery et al., 2013; Ralston and Ralston, 1994; Rausell et al., 1992; Vassias et al., 2005). Downregulation of GABA_ARs was linked to rapid somatotopic reorganization of the adult cortex after nerve injury, such as that underlying the unmasking of latent synaptic connections (Chen et al., 2002; Mowery et al., 2013; Ralston and Ralston, 1994; Rausell et al., 1992). GABA_ARs produce two types of inhibition: phasic and tonic. Phasic inhibition has fast kinetics and is mediated by synaptic GABA_ARs, whereas tonic inhibition has slower kinetics and is



mediated by extrasynaptic GABA_ARs. Extrasynaptic GABA_ARs are a key regulator of neural plasticity under normal and pathophysiological conditions (Collinson et al., 2002; Whissell et al., 2015). For instance, pharmacological inhibition or genetic knockdown of extrasynaptic GABA_ARs enhances long-term potentiation (Collinson et al., 2002). Reducing inordinate tonic inhibition is effective for recovery of motor function after a stroke in mice (Clarkson et al., 2010). In the thalamus, thalamocortical neurons receive GABAergic inhibition mainly from the reticular thalamic nucleus (Arcelli et al., 1997; Cox et al., 1997; Ohara and Lieberman, 1985; Steriade, 2005). Extrasynaptic GABA_ARs are highly expressed in the somatosensory thalamus (Belelli et al., 2005; Chandra et al., 2006; Jia et al., 2005; Peden et al., 2008) and regulate the excitability and firing mode of thalamocortical neurons (Cope et al., 2005). Moreover, Sametsky et al. (2015) reported that a peripheral acoustic insult upregulates extrasynaptic GABA_AR currents in the auditory thalamus. These results suggest that extrasynaptic GABA_ARs have a functional role in nerve injury-induced plasticity.

Here, we found that thalamic extrasynaptic GABA_AR currents were potentiated after injury to the whisker sensory nerve. Furthermore, potentiation of thalamic extrasynaptic GABA_AR currents induced remodeling of afferent fibers in the somatosensory thalamus and the development of ectopic mechanical hypersensitivity; both of which could be rescued by conditional deletion of thalamic extrasynaptic GABA_ARs. These results provide insights into the molecular basis of nerve injury-induced remodeling and associated phantom sensations.

RESULTS

Potentiation of Extrasynaptic GABA_AR Currents in the Ventral Posterior Medial Nucleus (VPM) of the Somatosensory Thalamus after Peripheral Nerve Injury

Somatosensory information from the whiskers is transferred to the principal trigeminal nucleus (PrV) via the infraorbital nerve (ION), the second branch of the trigeminal nerve. The information is then sent to neurons in the contralateral VPM through the medial lemniscal fibers, with each VPM neuron receiving input from a single fiber. We previously reported that an infraorbital nerve cut (IONC) in mice disrupts the normal, one-to-one connection of lemniscal fibers to VPM neurons, with recruitment of additional lemniscal fibers onto individual VPM neurons becoming apparent on approximately postoperative day 5 (POD5; Figure S1) (Takeuchi et al., 2012, 2017). Because each VPM neuron generally receives a single lemniscal fiber input, the lemniscal excitatory postsynaptic current (EPSC) is normally observed as an all-or-none response (a single-step EPSC) to increments of stimulus intensity applied to the lemniscal fibers. Following IONC, however, two or more discrete incremental EPSCs are elicited by lemniscal stimulation in approximately 70% of recorded VPM neurons (IONC-multiple neurons); the remaining 30% retain a single-step, all-or-none response (IONC-single neurons) as observed in normal VPM neurons. To investigate postoperative changes in tonic GABAergic inhibition after IONC, we recorded both lemniscal EPSCs (at a holding potential of -60 mV) and extrasynaptic GABA_AR currents (at a holding potential of 0 mV) from the same VPM neuron (see Method Details and Figure 1A). We first sequentially recorded agonist-

induced and endogenous extrasynaptic GABA_AR currents in VPM neurons. Application of an extrasynaptic GABA_AR agonist, THIP (Chandra et al., 2006; Peden et al., 2008) ($10 \mu\text{M}$ for 30 s), *in vitro* increased the holding current, reflecting extrasynaptic GABA_AR currents in VPM neurons (Figure 1B). The amplitude of agonist-induced extrasynaptic GABA_AR currents was larger in IONC neurons than it was in sham neurons on POD1–3 and thereafter (POD1–3, $p < 0.01$, unpaired Student's t test; POD4–5, $p < 0.05$, unpaired Student's t test; Figures 1B and 1C; Table S1). Interestingly, during POD6–9, we found that the agonist-induced potentiation of extrasynaptic GABA_AR currents was present in IONC-multiple neurons ($p < 0.01$, one-way ANOVA followed by Bonferroni test; Figures 1B and 1C; Table S1) but not in IONC-single neurons ($p > 0.05$ versus sham neurons; $p < 0.01$ versus IONC-multiple neurons; Figures 1B and 1C; Table S1).

We also evaluated endogenous extrasynaptic GABA_AR currents by measuring the differences in the holding currents before THIP application and during application of $100 \mu\text{M}$ of bicuculline methochloride, a GABA_AR antagonist. Consistent with the results from THIP application, during POD1–3, the mean amplitude was larger in IONC neurons than in sham neurons ($p < 0.05$, unpaired Student's t test; Figures 1B and 1D). This potentiation persisted during POD4–5 ($p < 0.05$, unpaired Student's t test; Figures 1B and 1D). During POD6–9, IONC-multiple neurons showed potentiation of endogenous extrasynaptic GABA_AR currents ($n = 15$, $p < 0.001$, one-way ANOVA followed by Bonferroni test) but not IONC-single neurons ($n = 11$, $p > 0.05$; Figures 1B and 1D), consistent with the results from THIP application. Next, we performed cluster analysis on endogenous and agonist-induced, extrasynaptic GABA_AR currents from all neurons, both IONC and sham. Neurons recorded during POD1–5 were classified as belonging to a small-amplitude cluster or a large-amplitude cluster (Figure S2). Although most of the sham neurons (94.1%, 16 of 17) belonged to the small-amplitude cluster, 66.7% (14 of 21) of the IONC neurons belonged to the large-amplitude cluster. The other IONC neurons (7 of 21) belonged to the small-amplitude cluster (Figure S2). These results suggest that the potentiation of extrasynaptic GABA_AR currents in VPM neurons after IONC correlates with the remodeling of lemniscal fibers in IONC-multiple neurons.

To assess whether an increase in GABA_AR expression underlies the IONC-induced potentiation of extrasynaptic GABA_AR currents, we examined the surface expression level of $\alpha 4$ subunits, a main component of extrasynaptic GABA_ARs in the VPM, and $\alpha 1$ subunits, a component of synaptic GABA_ARs (Peden et al., 2008) (Figure 2A). Cluster staining of $\alpha 4$ subunits was abundant near the soma and rarely colocalized with staining for $\alpha 1$ subunits (Figures 2B and 2C). IONC increased the number and area of $\alpha 4$ subunit immunoreactivity but had little effect on the number or area of $\alpha 1$ subunit immunoreactivity (Figures 2D–2G; Table S2). In IONC mice, there was little colocalization of $\alpha 4$ and $\alpha 1$ subunits (data not shown). Thus, these results suggest that an IONC-induced increase in $\alpha 4$ subunit expression underlies the potentiation of extrasynaptic GABA_AR currents in VPM neurons.

In contrast to the extrasynaptic GABA_AR currents, synaptic GABA_AR currents decreased in amplitude soon after IONC (Figure S3A). The amplitudes of evoked inhibitory postsynaptic currents (eIPSCs; Figures S3A and S3B), spontaneous IPSCs (sIPSCs; Figure S3C), and miniature IPSCs (mIPSCs; Figures

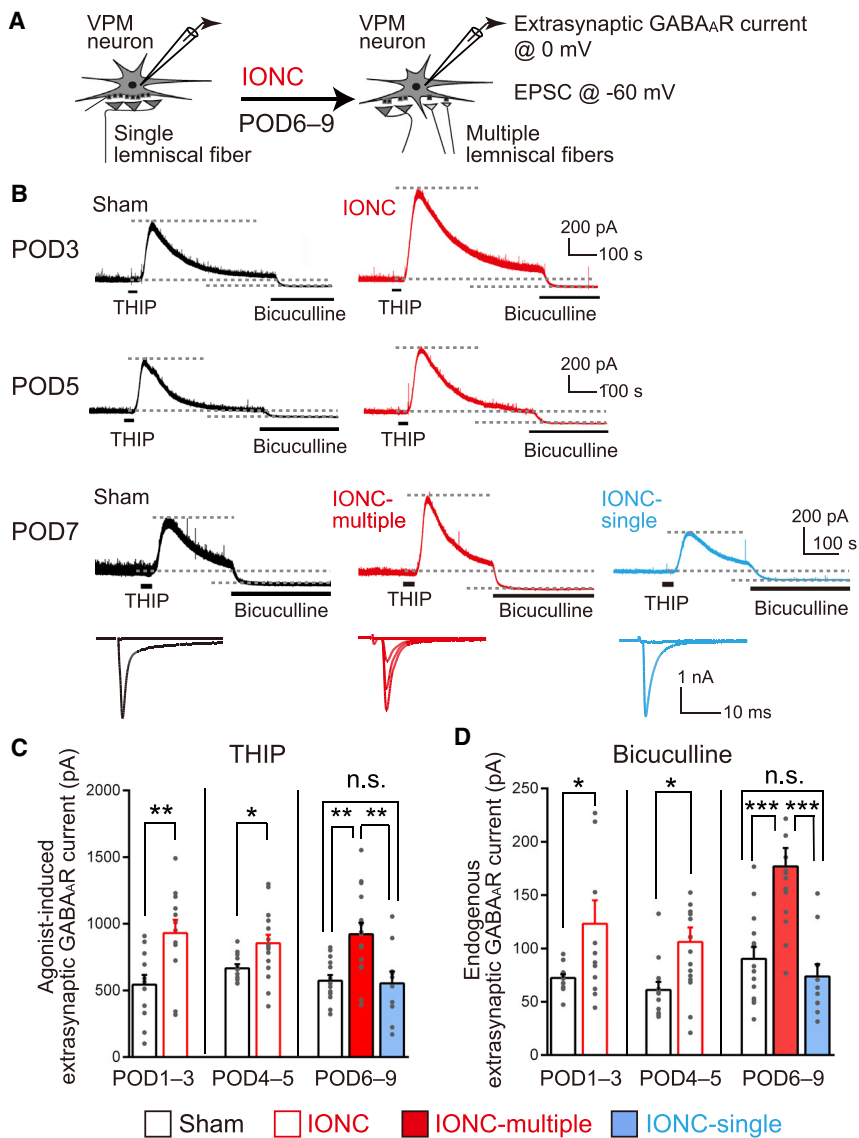


Figure 1. Infraorbital Nerve Cut (IONC) Markedly Increases Extrasynaptic GABA_{AR} Currents in a Ventral Posterior Medial Nucleus (VPM) Neuron

(A) Schematic drawings of the recording configuration and remodeling of the medial lemniscal fibers after IONC. AMPAR-mediated lemniscal EPSCs and extrasynaptic GABA_{AR} currents were recorded from the same neuron.

(B) Representative traces of extrasynaptic GABA_{AR} currents in VPM neurons of sham or IONC mice on postoperative day 3 (POD3) and POD5. Agonist-induced extrasynaptic GABA_{AR} currents are revealed by the shift in the holding current after application of THIP (extrasynaptic GABA_{AR} agonist; 10 μM, 30 s). Endogenous extrasynaptic GABA_{AR}s currents are estimated from the shift in the holding currents after application of bicuculline (GABA_{AR} antagonist; 100 μM, 5 min). Representative traces of AMPAR-mediated lemniscal EPSCs (bottom) and extrasynaptic GABA_{AR} currents (upper) in sham, IONC-multiple, and IONC-single neurons on POD7. (C and D) Summary graphs showing the mean amplitudes of agonist-induced or endogenous extrasynaptic GABA_{AR} currents with application of THIP (C) or bicuculline (D), respectively. Data represent the means ± SEM of 10–16 cells. *p < 0.05, **p < 0.01, ***p < 0.001, unpaired Student's t test or post hoc Bonferroni test after one-way ANOVA. n.s., not significant.

S3E and S3F) decreased from POD1 after IONC. During POD6–9, the sIPSC amplitudes were smaller in IONC-multiple neurons (eight neurons) than they were in sham neurons (seven neurons, p < 0.01, one-way ANOVA followed by Bonferroni test) or IONC-single neurons (seven neurons, p < 0.05; Figure S3C). The sIPSC frequencies in IONC neurons were decreased during POD1–3 (p < 0.001, unpaired Student's t test; Figure S3C), whereas the inter-event intervals of mIPSCs in IONC neurons did not differ from those in sham neurons (p > 0.05, Kolmogorov–Smirnov test; Figure S3G). During POD6–9, the sIPSC frequencies did not differ among the three groups (p > 0.05, one-way ANOVA; Figure S3D).

Inhibitory but Not Excitatory Charges Increase in VPM Neurons after Peripheral Nerve Injury

We further examined the excitatory and inhibitory charges in IONC neurons to estimate changes in excitatory and inhibitory

inputs (Figure 3A). In IONC-multiple neurons, although the phasic inhibitory charge was smaller than that in the sham neurons (p < 0.05, one-way ANOVA followed by Bonferroni test) or in IONC-single neurons (p < 0.05; Figures 3A and 3B; Table S3), the tonic inhibitory charge (Figure 3B; Table S3) and the total inhibitory charge (phasic plus tonic inhibitory charges; Figure 3C; Table S3) in IONC-multiple neurons were significantly larger than those in IONC-single neurons (tonic inhibitory charge, p < 0.001; total inhibitory charge, p < 0.001) and sham neurons (tonic inhibitory charge, p < 0.001; total inhibitory charge, p < 0.001). By contrast, the excitatory charge did not differ among the three groups (p > 0.05; Figure 3D; Table S3).

These results collectively indicate that the inhibitory charge was markedly potentiated in IONC neurons because of increased extrasynaptic GABA_{AR} currents, which were apparent as early as POD1, in advance of IONC-induced remodeling of the lemniscal afferents. Furthermore, this potentiation persisted to POD9 selectively in IONC-multiple neurons.

Activation of Extrasynaptic GABA_{AR}s Is Sufficient to Induce the Remodeling of Afferent Fibers

Our findings raise the possibility that potentiation of extrasynaptic GABA_{AR} currents may be sufficient to induce the remodeling of afferent fibers. To test that possibility, we infused THIP (100 μM) or saline continuously into the VPM of normal mice *in vivo* through

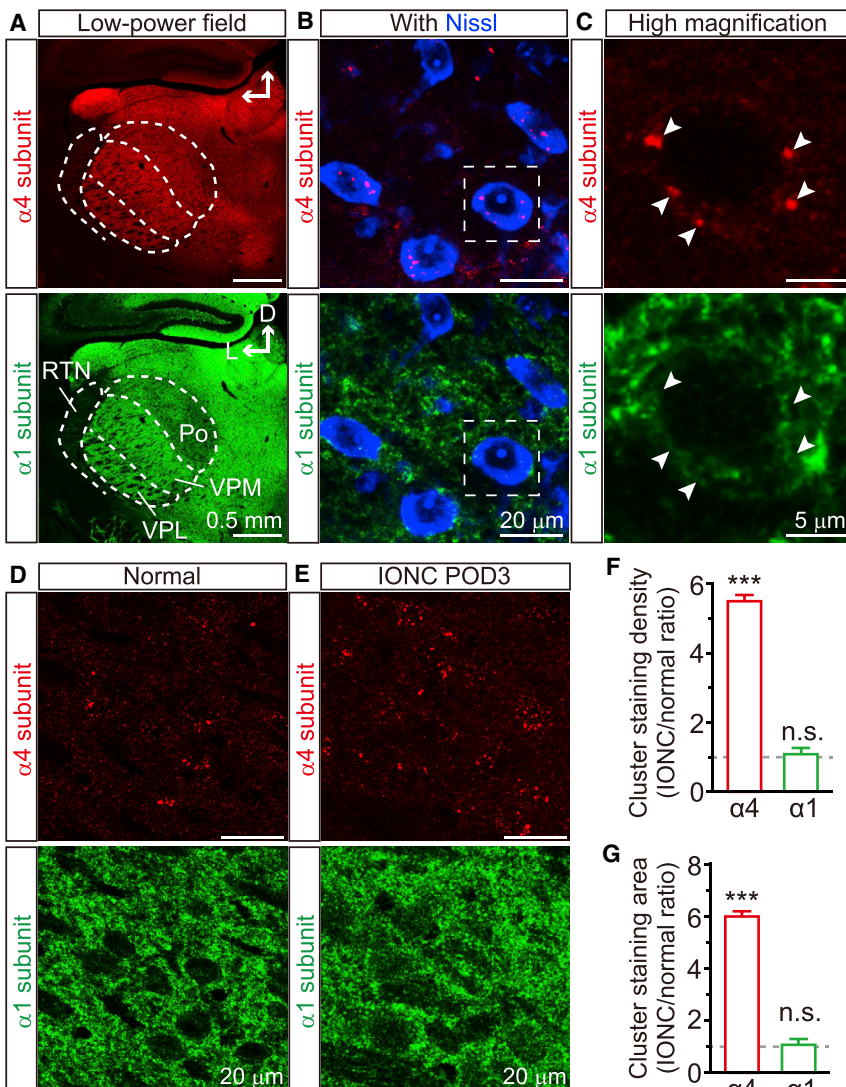


Figure 2. IONC Increases the Expression of Extrasynaptic GABA_AR α 4 Subunits in the VPM

(A) Immunohistochemical staining of α 4 (red) and α 1 (green) subunits in the VPM of a normal mouse at postnatal day (P24). D, dorsal; L, lateral; Po, posterior nucleus; RTN, reticular thalamic nucleus; VPL, ventral posterior lateral nucleus of the thalamus.

(B) Somatic localization of α 4 subunits (red) and ubiquitous distribution of α 1 subunits (green) in the VPM. The regions in the white, dotted boxes are magnified in (C).

(C) Segregation of α 4 (red) and α 1 (green) subunits at somatic location. Arrowheads, α 4 subunits that did not colocalize with α 1 subunits.

(D and E) Immunostaining of α 4 (red) and α 1 subunits (green) in normal (D) and IONC mice (E) at P24.

(F and G) Summary graphs showing the density (F) and area (G) of α 4- and α 1-immunoreactive clusters in the VPM of normal and IONC mice. Data are the means \pm SEM from three mice. ***p < 0.001 by unpaired Student's t test. n.s., not significant.

Extrasynaptic GABA_ARs in VPM Neurons Are Crucial for the Remodeling of Afferent Fibers after Peripheral Nerve Injury

If extrasynaptic GABA_ARs in the VPM are required for IONC-induced remodeling of lemniscal fibers, then the absence of extrasynaptic GABA_ARs in VPM neurons should prevent remodeling. To test that, we knocked out α 4 subunits from VPM neurons by injecting iCre-GFP-lentivirus into the VPM of P14 α 4-floxed mice (α 4 KO; see [Method Details](#)). We performed IONC on P21, 1 week after the lentivirus injection and recorded both lemniscal EPSCs and extrasynaptic GABA_AR currents from the same neurons during P28 to P33 ([Figure 5A](#)). The extrasynaptic GABA_AR current induced by a bath application of THIP (10 μ M) was almost entirely abolished in α 4 KO neurons, indicating that α 4 subunits were knocked out successfully ([Figure 5B](#)).

Under these conditions, the percentage of IONC-single neurons increased significantly to 62% (23 of 37) in α 4 KO neurons, compared with 25% (8 of 32) in control neurons ($p < 0.01$, χ^2 test; [Figure 5C](#)). In addition, this percentage of IONC-single neurons in α 4 KO mice did not differ from that in saline-treated mice ($p > 0.05$, χ^2 test; see [Figure 4C](#)). The mean amplitude of AMPAR-mediated, single-fiber lemniscal EPSCs was significantly larger in α 4 KO, than in control neurons ($p < 0.05$, unpaired Student's t test; [Figure 5D](#); [Table S4](#)). However, the mean maximum amplitude of AMPAR-mediated lemniscal EPSCs was not different ($p > 0.05$; [Figure 5E](#); [Table S4](#)). These results demonstrate that extrasynaptic GABA_ARs in VPM neurons are necessary for the IONC-induced remodeling of lemniscal fibers.

In contrast to the effect on remodeling, KO of the α 4 subunit had no effect on the eIPSC amplitude ($1,396 \pm 125$ pA for control

an osmotic mini-pump from postnatal day 21 (P21) and then recorded lemniscal EPSCs from P27 to P33 ([Figure 4A](#)). In saline-treated mice, only 23% (6 of 26) of the recorded VPM neurons received multiple lemniscal fiber inputs ([Figures 4B](#) and [4C](#)). By contrast, the proportion of neurons that received multiple inputs was significantly increased to 57% (16 of 28) in THIP-treated mice ($p < 0.05$, χ^2 test; [Figures 4B](#) and [4C](#)). These results indicate that activation of extrasynaptic GABA_ARs is sufficient to induce the remodeling of lemniscal fibers. The mean amplitude of α -amino-3-hydroxy-5-methylisoxazole-4-propionate receptor (AMPAR)-mediated, single-fiber lemniscal EPSCs in THIP-treated neurons was significantly smaller than it was in saline-treated neurons ($p < 0.05$, unpaired Student's t test; [Figure 4D](#); [Table S4](#)). However, the maximum amplitude of AMPAR-mediated lemniscal EPSCs was not affected by THIP treatment ($p > 0.05$; [Figure 4E](#); [Table S4](#)). These results closely resemble those reported in our previous study of IONC-induced remodeling of lemniscal fibers ([Takeuchi et al., 2012](#)).

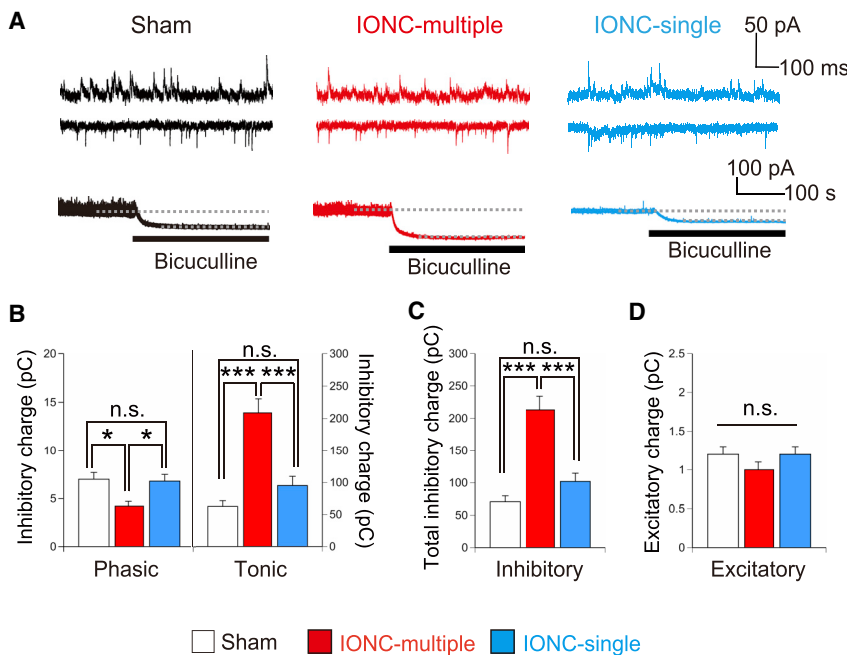


Figure 3. IONC Potentiates the Inhibitory Charge Specifically in VPM Neurons with Abnormally Recruited Lemniscal Fibers

(A) Representative traces of spontaneous sIPSCs (top), spontaneous sEPSCs (middle), and extrasynaptic GABA_AR currents (revealed by bicuculline, bottom) in sham, IONC-multiple, and IONC-single neurons on POD7.

(B–D) Summary graphs showing the mean inhibitory phasic and tonic charges (B), the total inhibitory charges (phasic plus tonic) (C), and the excitatory charges (D) of sIPSCs, extrasynaptic GABA_AR currents, and sEPSCs during POD6–9. The tonic charge was calculated from the extrasynaptic GABA_AR currents revealed by application of bicuculline (100 μM). Data represent the means ± SEM of seven to eight cells. *p < 0.05, p < 0.001, post hoc Bonferroni test after one-way ANOVA. n.s., not significant.

neurons, n = 11 versus 1,713 ± 264 pA for α4 KO neurons, n = 12; p > 0.05, unpaired Student's t test). Furthermore, the sIPSC amplitude in α4 KO neurons was not altered by bath application of THIP (p > 0.05, paired Student's t test; Figure S4). Therefore, our findings are consistent with previous reports that the phasic IPSCs are not affected by the deletion of α4 subunits (Chandra et al., 2006) or the application of THIP (Belelli et al., 2005; Sametsky et al., 2015).

Extrasynaptic GABA_ARs Also Contribute to the Maintenance of the Remodeling

We previously demonstrated that IONC induces remodeling of lemniscal fibers from POD5 (Takeuchi et al., 2012, 2017). We found that potentiated extrasynaptic GABA_AR currents persisted selectively in IONC-multiple neurons (POD6–9; Figure 1). This raises the possibility that extrasynaptic GABA_ARs contribute to the maintenance of the remodeling, as well as its induction. To test that possibility, we knocked out α4 subunits after remodeling in the VPM (Figure 6A). Lentivirus vector expressing iCre-GFP was injected into the VPM at P26 (POD5) to delete α4 subunits during P33–43 (POD12–22; Figure 6A). From 1 week after the lentivirus injection (on P33–43), we recorded lemniscal EPSCs from both α4 KO and control neurons (Figures 6A and 6B). Approximately 67% (20 of 30) of the control neurons received multiple fiber inputs (IONC-multiple neurons; Figures 6C and 6D). By contrast, in α4 KO neurons, the percentage of IONC-multiple neurons was markedly decreased to 24% (4 of 17 recorded neurons, p < 0.05, χ² test; Figures 6C and 6D). Moreover, there was no significant difference in the mean amplitude of AMPAR-mediated, single-fiber lemniscal EPSCs between α4 KO and control neurons (p > 0.05, unpaired Student's t test; Figure 6E; Table S4). However, the mean maximum amplitudes were significantly smaller in α4 KO neurons than they were in control neurons (p < 0.05; Figure 6F; Table S4), suggesting that deletion of α4 eliminated the

surplus fibers, but the synaptic strength of the weakened remaining fibers after IONC was insufficient to recover the original maximal amplitude. Together, these results

indicate that extrasynaptic GABA_ARs are involved not only in the induction but also in the maintenance of afferent fiber remodeling in VPM neurons after IONC.

Change in VPM Neuronal Activity after Peripheral Nerve Injury

Several lines of evidence indicate that activity in VPM neurons is influenced by GABAergic inhibition (Cope et al., 2005). Relative hyperpolarization by GABAergic inhibition de-inactivates T-type Ca²⁺ channels, inducing burst-mode firing (Sherman, 2001). We observed that potentiation of extrasynaptic GABA_AR currents by bath application of THIP *in vitro* hyperpolarized the membrane potential and changed the cell firing pattern from tonic to burst (Figure S5). Therefore, it is possible that the potentiation of extrasynaptic GABA_AR currents after IONC influences the firing pattern of VPM neurons *in vivo*. To test that possibility, we recorded spontaneous spikes from the barrelloid area of the VPM in awake head-fixed mice after IONC (Figures S6). During POD9–10, the tonic spike frequency decreased significantly (p < 0.05; Figures S6F and S6G), but the burst spike frequency did not change (p > 0.05, Mann-Whitney U test), and the total spike frequency (tonic and burst) decreased with IONC (p < 0.05, Mann-Whitney U test; Figures S6F and S6G). Consequently, the proportion of burst spikes to total spikes increased significantly (p < 0.01; Figure S6H). These results suggest that, after IONC, VPM neuronal firing was globally inhibited by the increased tonic inhibitory conductance and shifted from tonic- to burst-firing mode *in vivo*.

Thalamic Tonic GABA_AR Inhibition Controls Peripheral Nerve Injury-Induced Ectopic Mechanical Hypersensitivity

We previously reported that the origins of the newly recruited afferent fibers after IONC include the V3 subregion of the

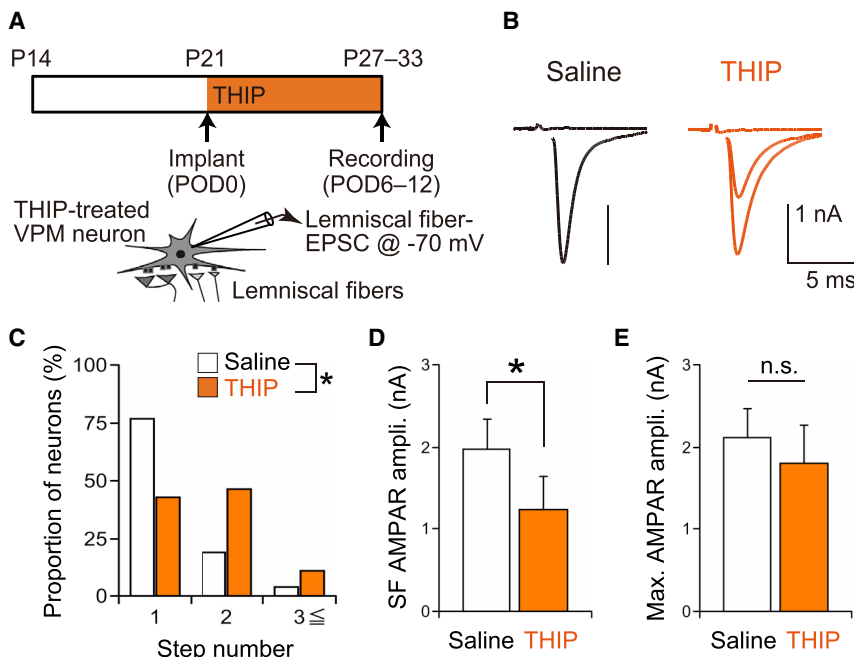


Figure 4. Chronic Treatment with an Extrasynaptic GABA_AR Agonist *In Vivo* Recruits Additional Lemniscal Fibers to VPM Neurons

(A) Experimental schedule.

(B) Representative traces of AMPAR-mediated lemniscal EPSCs from VPM neurons in slices prepared from saline- or 100- μ M THIP-treated mice.

(C) Proportions of VPM neurons with different numbers of discrete lemniscal EPSC steps in saline- and THIP-treated mice. The number of recorded neurons was 26–28. * $p < 0.05$ by χ^2 test.

(D and E) Summary bar graphs showing the mean amplitudes of single fiber (SF)-mediated lemniscal EPSCs (D) and maximum (Max.) lemniscal EPSCs (E) at a holding potential of -70 mV. Data represent the means \pm SEM of 20–25 neurons. * $p < 0.05$ by unpaired Student's t test. n.s., not significant.

trigeminal nuclei (PrV3) and the cuneate nucleus, which carry somatosensory information from the mandibular (lower jaw) region and other areas of the body, respectively (Takeuchi et al., 2017). Concomitant with these changes, mice show allodynia-like ectopic mechanical hypersensitivity in the mandibular region adjacent to the injured maxillary (whisker pad) region after IONC (Takeuchi et al., 2017).

To confirm whether potentiated extrasynaptic GABA_AR currents after IONC are involved in the ectopic mechanical hypersensitivity observed after IONC, we examined IONC-induced ectopic mechanical hypersensitivity in $\alpha 4$ KO mice (Figure 7). Using the von Frey test, we measured withdrawal thresholds in response to mechanical stimulation applied to the mandibular or maxillary region before (P21) and after (POD4–5) IONC (Figures 7A and 7B). As we reported previously (Takeuchi et al., 2017), IONC causes ectopic hypersensitivity: the withdrawal threshold for the ipsilateral mandibular region was lower after IONC in control mice ($p < 0.001$, one-way ANOVA followed by Bonferroni test; Figure 7C; Table S5). However, in $\alpha 4$ KO mice, this ectopic hypersensitivity was significantly suppressed, as demonstrated by recovery of the withdrawal threshold in $\alpha 4$ KO mice ($p < 0.001$; Figure 7C; Table S5). There was no withdrawal response (i.e., mice did not respond even at the maximum cutoff force) to stimulation of the maxillary region in either control or $\alpha 4$ KO mice ($p < 0.001$; Figure 7C; Table S5) because those mice had no abnormal sensation in the maxillary region after IONC. When a sham operation was performed instead of IONC, the withdrawal thresholds in control and $\alpha 4$ KO mice were unaffected (Figures S7A–S7C).

In addition, THIP infusion into the center of the barrelloid of the VPM was sufficient to induce mechanical hypersensitivity in the contralateral mandibular region in normal mice (Figures S7D–S7F). We observed a reduction in the withdrawal threshold in

the left mandibular region with THIP treatment, relative to both the pre-treatment withdrawal threshold ($p < 0.001$; Figure S7F) and saline controls ($p < 0.01$; Figure S7F). We also observed that the threshold tended to decrease for the contralateral maxillary region in THIP-treated mice, although the effect was not significant ($p > 0.05$, one-way ANOVA followed by Bonferroni test; Figure S7F). This tendency was probably due to drug diffusion. Taken together, these results strongly suggest that potentiated extrasynaptic GABA_AR activation is critically involved in IONC-induced ectopic mechanical hypersensitivity.

DISCUSSION

GABAergic inhibition has been implicated in multiple aspects of the plasticity that occurs in the CNS following peripheral nerve injury. In the present study, we show that extrasynaptic GABA_ARs are crucial for triggering and maintaining the abnormal remodeling of afferent fibers in the VPM after peripheral nerve injury and for the resulting ectopic sensations.

Peripheral nerve injury or deafferentation leads to changes in the expression levels of GABA, GAD, and GABA_ARs in the spinal cord (Castro-Lopes et al., 1993; Fukuoka et al., 1998; Moore et al., 2002), brainstem (Vassias et al., 2005), thalamus (Ralston and Ralston, 1994; Rausell et al., 1992), and cerebral cortex (Garraghty et al., 1991; Hendry and Jones, 1986; Jones and Pons, 1998; Mowery et al., 2013; Welker et al., 1989). We previously reported that IONC induces remodeling of lemniscal fibers from POD5 (Takeuchi et al., 2012). Here, extrasynaptic GABA_AR currents in VPM neurons were potentiated soon after IONC (from POD1), before the remodeling. This potentiation continued and was detected at POD6–9 selectively in VPM neurons that exhibited remodeling of lemniscal fibers. Interestingly, neurons recorded during POD1–5 could be divided into two clusters, with and without potentiation of extrasynaptic GABA_AR currents, even before the remodeling occurred. The proportion of neurons in the potentiated cluster was very similar to that of the remodeled neurons (about 70%). These results strongly suggest that

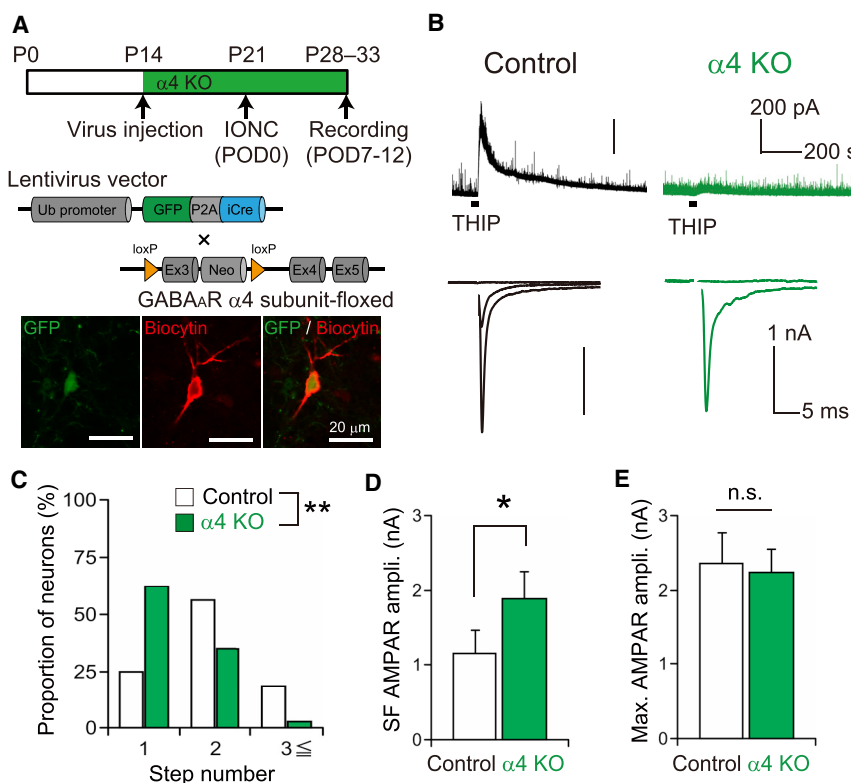


Figure 5. Conditional Deletion of Extrasynaptic GABA_AR $\alpha 4$ Subunits from VPM Neurons before IONC Prevents IONC-Induced Remodeling of Lemniscal Afferent Fibers

(A) Top: experimental schedule. Middle: lentivirus vector design and gene structure of $\alpha 4$ -floxed mice. Injection of lentivirus vector into the VPM of $\alpha 4$ -floxed mice induces excision of the exon 3 domain of the $\alpha 4$ subunit. Bottom: representative images from a whole-cell-recorded neuron expressing GFP (green) and filled with biocytin (red) in the VPM.

(B) Top: extrasynaptic GABA_AR currents in a VPM neuron are abolished by knockout of $\alpha 4$ subunits ($\alpha 4$ KO neurons). Bottom: representative traces of AMPAR-mediated lemniscal EPSCs in control (left) and $\alpha 4$ KO (right) neurons.

(C) Proportions of $\alpha 4$ KO and control VPM neurons with different numbers of discrete AMPAR-mediated lemniscal EPSC steps. The number of recorded neurons was 32–37. * $p < 0.05$ by χ^2 test. (D and E) Summary bar graphs showing the mean amplitudes of AMPAR-mediated SF lemniscal EPSCs (D) and Max. lemniscal EPSCs (E). Data represent the means \pm SEM of 34–36 neurons. * $p < 0.05$ by unpaired Student's t test. n.s., not significant.

potentiation of extrasynaptic GABA_AR activation determines whether the neuron will be remodeled or not. Moreover, pharmacological activation of thalamic extrasynaptic GABA_ARs in normal mice induced the recruitment of new lemniscal fibers, resembling IONC-induced remodeling, and conditional knockout of extrasynaptic GABA_ARs in the VPM prevented the remodeling of lemniscal fibers. Interestingly, deletion of extrasynaptic GABA_ARs at a later stage rescued the remodeling (Figure 6). Taken together, these results indicate that potentiation of extrasynaptic GABA_ARs is an indispensable factor in triggering the remodeling and is also crucial for the maintenance of the remodeled network.

Clarkson et al. (2010) demonstrated that a reduction in GABA uptake from GABA transporter dysfunction contributes to enhanced tonic inhibition in the peri-infarct cortex after a stroke. Although we did not rule out a possible contribution of GABA transporters to the enhanced GABA_AR current in our study, we did find that the expression of extrasynaptic GABA_ARs was markedly increased after IONC (Figure 2) and that the currents were enhanced by direct activation of extrasynaptic GABA_ARs by THIP (Figure 1). Therefore, the potentiation of extrasynaptic GABA_AR currents was likely caused by an increased number of extrasynaptic GABA_ARs on VPM neurons, rather than by changes in the GABA transporter function.

It was reported that GABA can exert an excitatory effect after peripheral injury in the spinal cord and the cortex because of the downregulation of K⁺-Cl⁻ cotransporter 2 (KCC2) (Coull et al., 2003; Mòdol et al., 2014). However, any such influence on the

activity of VPM neurons appears to be relatively minor in the present study because of the burst-firing mode observed *in vitro*, which generally occurs in hyperpolarized VPM neurons (Figure S5) (Cope et al., 2005). Postsynaptic excitability has a critical role in the development of innervation patterns (Lorenzetto et al., 2009; Mikuni et al., 2013). For instance, a genetic reduction of neural activity in postsynaptic cerebellar Purkinje cells impairs the normal one-to-one connection between presynaptic climbing fibers and Purkinje cells (Lorenzetto et al., 2009; Mikuni et al., 2013). Thus, we argue that the reduced excitability of VPM neurons caused by potentiated extrasynaptic GABA_AR currents drives the abnormal remodeling of afferent fibers.

It has been proposed that changes in synaptic and extrasynaptic GABA_AR subunits can be compensatory (Drexel et al., 2013; Liang et al., 2004; Zhang et al., 2007). For instance, overexpression of extrasynaptic GABA_ARs decreases synaptic GABA_AR transmission in mouse hippocampal neurons (Wu et al., 2013). This suggests that synaptic and extrasynaptic GABA_ARs compete for a limited number of receptor slots on a neuron. Cortical lesions also induce enhanced extrasynaptic GABA_AR currents but reduce synaptic GABA_AR currents (Imbrosi et al., 2013). Similar homeostatic mechanisms may occur in the VPM in the present study after peripheral nerve injury. However, regarding the remodeling, potentiation of extrasynaptic GABA_AR currents is likely to be the primary process because solitary application of an extrasynaptic GABA_AR agonist, THIP, mimicked IONC-induced remodeling without any effect on synaptic GABA_AR currents (Figures 4 and S4).

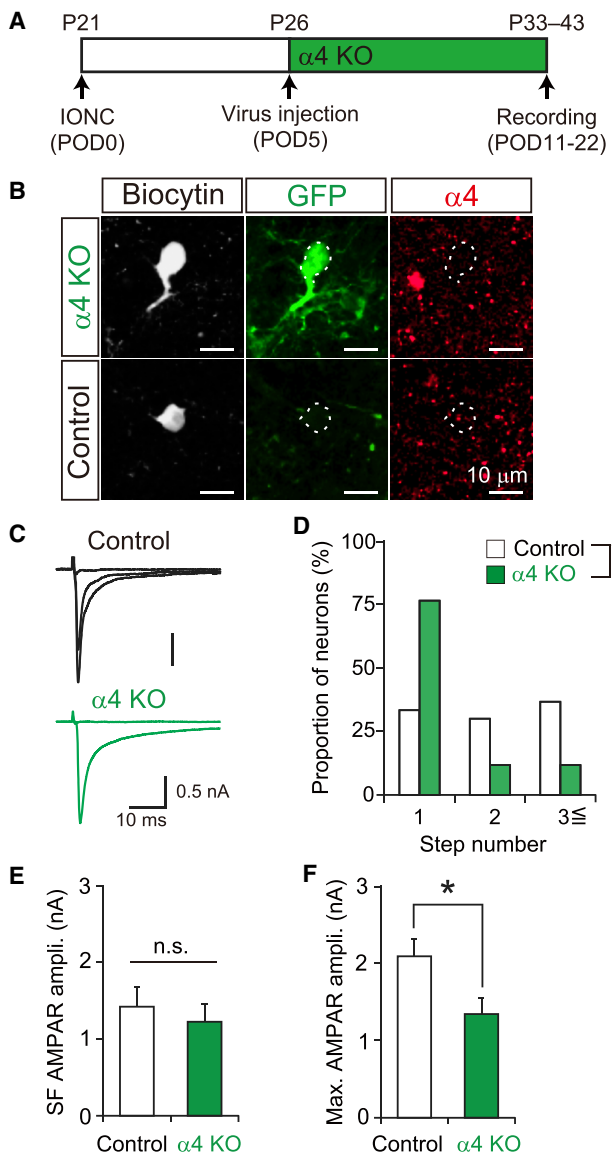


Figure 6. Conditional Deletion of Extrasynaptic GABA_AR α4 Sub-units from VPM Neurons after IONC Restores IONC-Induced Remodeling of Lemniscal Afferent Fibers

(A) Experimental schedule. IONC was conducted at P21 (POD0) in α4-floxed mice and lentivirus vector expressing improved Cre (iCre), and GFP was injected into the VPM at P26 (POD5). Lemniscal afferent fiber-EPSCs were recorded from α4 KO (GFP-positive) and neighboring control (GFP-negative) VPM neurons during P33–43 (POD11–22).

(B) Images of a recorded VPM neuron expressing GFP (top, α4 KO, green) and a recorded neuron that did not express GFP (bottom, control). The neurons were filled with biocytin (white) and immunostained with an anti-α4 subunit antibody (red).

(C) Representative traces of AMPAR-mediated lemniscal EPSCs from a control neuron (top) and an α4 KO neuron (bottom).

(D) Proportions of α4 KO and control VPM neurons with different numbers of discrete AMPAR-mediated lemniscal EPSC steps. The number of recorded neurons was 17–30. *p < 0.05 by χ^2 test.

(E and F) Summary bar graphs showing the mean amplitudes of SF (E) and Max. (F) AMPAR-mediated EPSCs. Data represent the means ± SEM of 17–30 neurons. *p < 0.05 by unpaired Student's t test. n.s., not significant.

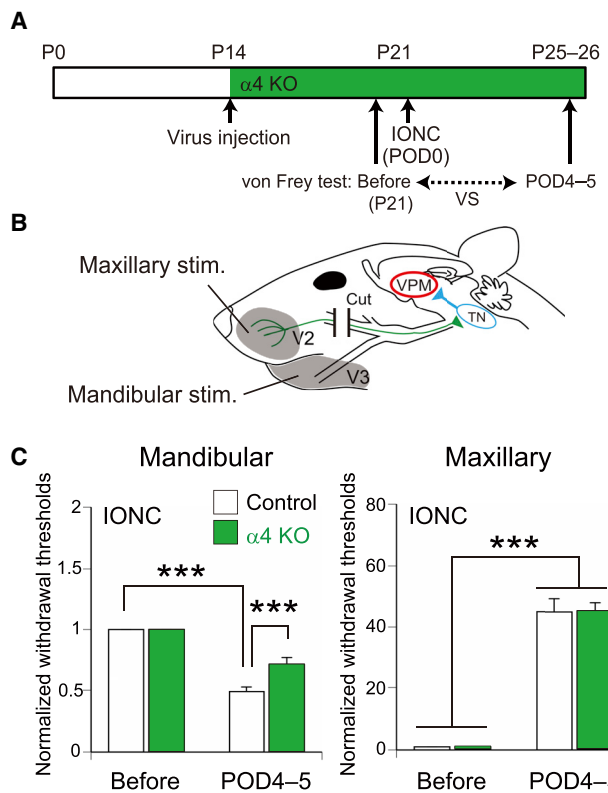


Figure 7. Conditional Deletion of Extrasynaptic GABA_AR α4 Sub-units Suppresses Ectopic Mechanical Hypersensitivity in the Mandibular Region of Mice

(A) Experimental schedule for behavioral tests with lentivirus-vector-injected α4-floxed mice.

(B) Schematic drawing of mechanical stimulation area and surgical operation.

(C) Summary bar graphs showing the changes in the mechanical withdrawal threshold induced by IONC on the ipsilateral side of the mandibular (left) and maxillary (right) regions. Data represent the means ± SEM of 10–12 mice. ***p < 0.001, post hoc Bonferroni test after one-way ANOVA.

Clinical deafferentation of peripheral sensory inputs, such as limb amputation, frequently leads to neuropathic pain, including phantom referred pain. Although the pathophysiological mechanisms underpinning these abnormal sensations are not fully understood, it was proposed that reorganization of neural circuits in the somatosensory thalamus is the primary cause (Head and Holmes, 1911; Ray et al., 2009). Several intraoperative studies revealed that somatotopic rearrangement is well correlated with phantom pain. We recently reported that IONC leads to ectopic mechanical hypersensitivity in the mandibular region (Takeuchi et al., 2017), which is innervated by the third branch of the trigeminal nerve, consistent with previously reported pain behavior (Iwata et al., 2001; Nomura et al., 2002; Tal and Bennett, 1994; Tsuboi et al., 2004). We further reported that the anatomical and functional remodeling of lemniscal fibers closely correlates with reorganization of the receptive field and ectopic mechanical hypersensitivity (Takeuchi et al., 2017). The origins of these newly recruited fibers after IONC are the unaffected ectopic regions: the mandibular principal trigeminal

nucleus, the interpolar part of the spinal trigeminal nucleus, and the dorsal column nuclei (Takeuchi et al., 2017). This somatotopic reorganization is well matched to the body parts with ectopic mechanical hypersensitivity. Here, we demonstrated that extrasynaptic GABA_AR currents in the VPM are required for the abnormal remodeling of lemniscal fibers and regulated ectopic mechanical hypersensitivity in the mandibular region. Therefore, the abnormal remodeling of lemniscal fibers induced by the potentiation of tonic GABA_AR inhibition presumably drives the ectopic mechanical hypersensitivity.

We also observed that VPM neuronal firing shifted to burst mode *in vivo* after IONC (Figure S6), which is consistent with the potentiation of extrasynaptic GABA_AR currents. Burst discharges in the somatosensory thalamus are proposed to be related to neuropathic pain (Hains et al., 2005, 2006; LeBlanc et al., 2016; Lenz et al., 1989, 1998). For instance, an abnormal bursting pattern is observed in the thalamic neurons of patients with neuropathic pain, including phantom pain (Lenz et al., 1989, 1993, 1998; Radhakrishnan et al., 1999), and in animals after nerve damage (LeBlanc et al., 2016; Wang and Thompson, 2008; Weng et al., 2000). In contrast, there have been conflicting reports that thalamic bursts negatively correlate with pain (Huh and Cho, 2013; Radhakrishnan et al., 1999). Therefore, the role of burst discharges in pain behavior remains controversial. More research will be required to show definitely that burst discharges are responsible for ectopic hypersensitivity.

Multiple lines of evidence demonstrate the alteration of extrasynaptic GABA_AR function under pathological conditions, including tinnitus (Sametsky et al., 2015), alcoholism (Follesø et al., 2005), epilepsy (Peng et al., 2004), depression (Holm et al., 2011), and traumatic brain injury (Kharlamov et al., 2011). For instance, a peripheral acoustic insult upregulates extrasynaptic GABA_AR currents in the auditory thalamus (Sametsky et al., 2015). Clarkson et al. (2010) previously found that genetically reducing the number of extrasynaptic GABA_ARs proved beneficial for functional recovery after a stroke. Together with our findings, these previous studies suggest that potentiated extrasynaptic GABA_AR currents after peripheral nerve injury have a critical role in the pathological, plastic changes in the CNS. Importantly, we demonstrate here that blockade of extrasynaptic GABA_AR currents in the somatosensory thalamus rescues abnormal remodeling of lemniscal fibers and ectopic mechanical hypersensitivity after peripheral nerve injury. Therefore, control of potentiated extrasynaptic GABA_ARs currents in the somatosensory thalamus may be an effective therapeutic strategy for phantom and/or referred pain.

STAR★METHODS

Detailed methods are provided in the online version of this paper and include the following:

- **KEY RESOURCES TABLE**
- **RESOURCE AVAILABILITY**
 - Lead Contact
 - Materials availability
 - Data and code availability

● EXPERIMENTAL MODEL AND SUBJECT DETAILS

- Animals
 - Complete transection of ION
- **METHOD DETAILS**
 - Slice preparation
 - *In vitro* whole-cell recordings
 - Immunohistochemical staining of α subunits of the GABA_AR
 - Chronic administration of an extrasynaptic GABA_AR agonist through an osmotic mini-pump
 - Virus preparation and infection
 - *In vivo* extracellular recording of thalamic neuronal firing in unanesthetized mice
 - Tactile sensory test

● QUANTIFICATION AND STATISTICAL ANALYSIS

SUPPLEMENTAL INFORMATION

Supplemental Information can be found online at <https://doi.org/10.1016/j.celrep.2020.107797>.

ACKNOWLEDGMENTS

This work was supported by JSPS KAKENHI grant numbers 24790580 (to Y.N.), 15K19195 (to Y.N.), 23500400 (to M.M.), 26290010 (to M.M.), 16K18995 (to Y.U.), 25000015 (to M.K.), 15H01667 (to M.M.), 16H01344 (to M.M.), 17H05752 (to M.M.), 17H05912 (to H.O.), 17K07058 (to H.N.), 18H04012 (to M.K.), 19H03343 (to M.M.), 20K06862 (to H.N.) and 20H05481 (to M.M.); the JST PRESTO Grant Japan, the Aya Irisawa Memorial promotion award, SHISEIKAI scholarship fund for basic researcher of medical science, and the Keiko Watanabe award (to M.M.) and the Narishige Neuroscience Research Foundation (to Y.U.). We thank Dr. S. Chiken and Prof. A. Nambu for technical advice on *in vivo* recording.

AUTHOR CONTRIBUTIONS

Y.N. and M.M. designed the study; Y.N., Y.U., H.N., Y.T., and H.O. conducted the experiments; Y.N., Y.U., H.N., Y.T., H.O., and M.M. analyzed the data; N.U. and M.K. provided the viral vector and helpful feedback on the manuscript; and Y.N. and M.M. wrote the paper.

DECLARATION OF INTERESTS

The authors declare no competing interests.

Received: April 18, 2018

Revised: March 10, 2020

Accepted: June 1, 2020

Published: June 23, 2020

REFERENCES

- Arcelli, P., Frassoni, C., Regondi, M.C., De Biasi, S., and Spreafico, R. (1997). GABAergic neurons in mammalian thalamus: a marker of thalamic complexity? *Brain Res. Bull.* 42, 27–37.
- Arsenault, D., and Zhang, Z.W. (2006). Developmental remodelling of the lemniscal synapse in the ventral basal thalamus of the mouse. *J. Physiol.* 573, 121–132.
- Belelli, D., Peden, D.R., Rosahl, T.W., Wafford, K.A., and Lambert, J.J. (2005). Extrasynaptic GABA_A receptors of thalamocortical neurons: a molecular target for hypnotics. *J. Neurosci.* 25, 11513–11520.
- Castro-Lopes, J.M., Tavares, I., and Coimbra, A. (1993). GABA decreases in the spinal cord dorsal horn after peripheral neurectomy. *Brain Res.* 620, 287–291.

- Chandra, D., Jia, F., Liang, J., Peng, Z., Suryanarayanan, A., Werner, D.F., Spigelman, I., Houser, C.R., Olsen, R.W., Harrison, N.L., and Homanics, G.E. (2006). GABA_A receptor α 4 subunits mediate extrasynaptic inhibition in thalamus and dentate gyrus and the action of gaboxadol. *Proc. Natl. Acad. Sci. USA* **103**, 15230–15235.
- Chen, R., Cohen, L.G., and Hallett, M. (2002). Nervous system reorganization following injury. *Neuroscience* **111**, 761–773.
- Chiken, S., Shashidharan, P., and Nambu, A. (2008). Cortically evoked long-lasting inhibition of pallidal neurons in a transgenic mouse model of dystonia. *J. Neurosci.* **28**, 13967–13977.
- Clarkson, A.N., Huang, B.S., Macisaac, S.E., Mody, I., and Carmichael, S.T. (2010). Reducing excessive GABA-mediated tonic inhibition promotes functional recovery after stroke. *Nature* **468**, 305–309.
- Collinson, N., Kuenzi, F.M., Jarolimek, W., Maubach, K.A., Cothliff, R., Sur, C., Smith, A., Otu, F.M., Howell, O., Atack, J.R., et al. (2002). Enhanced learning and memory and altered GABAergic synaptic transmission in mice lacking the α 5 subunit of the GABA_A receptor. *J. Neurosci.* **22**, 5572–5580.
- Cope, D.W., Hughes, S.W., and Crunelli, V. (2005). GABA_A receptor-mediated tonic inhibition in thalamic neurons. *J. Neurosci.* **25**, 11553–11563.
- Coull, J.A., Boudreau, D., Bachand, K., Prescott, S.A., Nault, F., Sik, A., De Koninck, P., and De Koninck, Y. (2003). Trans-synaptic shift in anion gradient in spinal lamina I neurons as a mechanism of neuropathic pain. *Nature* **424**, 938–942.
- Cox, C.L., Huguenard, J.R., and Prince, D.A. (1997). Nucleus reticularis neurons mediate diverse inhibitory effects in thalamus. *Proc. Natl. Acad. Sci. USA* **94**, 8854–8859.
- Dixon, W.J. (1980). Efficient analysis of experimental observations. *Annu. Rev. Pharmacol. Toxicol.* **20**, 441–462.
- Drexel, M., Kirchmair, E., and Sperk, G. (2013). Changes in the expression of GABA_A receptor subunit mRNAs in parahippocampal areas after kainic acid induced seizures. *Front. Neural Circuits* **7**, 142.
- Eto, K., Wake, H., Watanabe, M., Ishibashi, H., Noda, M., Yanagawa, Y., and Nabekura, J. (2011). Inter-regional contribution of enhanced activity of the primary somatosensory cortex to the anterior cingulate cortex accelerates chronic pain behavior. *J. Neurosci.* **31**, 7631–7636.
- Follesa, P., Mostallino, M.C., Biggio, F., Gorini, G., Caria, S., Busonero, F., Murru, L., Mura, M.L., Sanna, E., and Biggio, G. (2005). Distinct patterns of expression and regulation of GABA receptors containing the δ subunit in cerebellar granule and hippocampal neurons. *J. Neurochem.* **94**, 659–671.
- Franklin, K.B.J., and Paxinos, G. (2007). *The Mouse Brain in Stereotaxic Coordinates*, Third Edition (Academic Press).
- Fukuoka, T., Tokunaga, A., Kondo, E., Miki, K., Tachibana, T., and Noguchi, K. (1998). Change in mRNAs for neuropeptides and the GABA_A receptor in dorsal root ganglion neurons in a rat experimental neuropathic pain model. *Pain* **78**, 13–26.
- Garraghty, P.E., LaChica, E.A., and Kaas, J.H. (1991). Injury-induced reorganization of somatosensory cortex is accompanied by reductions in GABA staining. *Somatosens. Mot. Res.* **8**, 347–354.
- Graziano, A., and Jones, E.G. (2009). Early withdrawal of axons from higher centers in response to peripheral somatosensory denervation. *J. Neurosci.* **29**, 3738–3748.
- Hains, B.C., Saab, C.Y., and Waxman, S.G. (2005). Changes in electrophysiological properties and sodium channel Na_v1.3 expression in thalamic neurons after spinal cord injury. *Brain* **128**, 2359–2371.
- Hains, B.C., Saab, C.Y., and Waxman, S.G. (2006). Alterations in burst firing of thalamic VPL neurons and reversal by Na_v1.3 antisense after spinal cord injury. *J. Neurophysiol.* **95**, 3343–3352.
- Head, H., and Holmes, G. (1911). Sensory disturbances from cerebral lesions. *Brain* **34**, 102–254.
- Hendry, S.H., and Jones, E.G. (1986). Reduction in number of immunostained GABAergic neurones in deprived-eye dominance columns of monkey area 17. *Nature* **320**, 750–753.
- Holm, M.M., Nieto-Gonzalez, J.L., Vardya, I., Henningsen, K., Jayatissa, M.N., Wiborg, O., and Jensen, K. (2011). Hippocampal GABAergic dysfunction in a rat chronic mild stress model of depression. *Hippocampus* **21**, 422–433.
- Huh, Y., and Cho, J. (2013). Discrete pattern of burst stimulation in the ventrobasal thalamus for anti-nociception. *PLoS ONE* **8**, e67655.
- Huntsman, M.M., and Huguenard, J.R. (2000). Nucleus-specific differences in GABA_A-receptor-mediated inhibition are enhanced during thalamic development. *J. Neurophysiol.* **83**, 350–358.
- Imbroisci, B., Neubacher, U., White, R., Eysel, U.T., and Mittmann, T. (2013). Shift from phasic to tonic GABAergic transmission following laser-lesions in the rat visual cortex. *Pflugers Arch.* **465**, 879–893.
- Iwata, K., Imai, T., Tsuboi, Y., Tashiro, A., Ogawa, A., Morimoto, T., Masuda, Y., Tachibana, Y., and Hu, J. (2001). Alteration of medullary dorsal horn neuronal activity following inferior alveolar nerve transection in rats. *J. Neurophysiol.* **86**, 2868–2877.
- Jia, F., Pignataro, L., Schofield, C.M., Yue, M., Harrison, N.L., and Goldstein, P.A. (2005). An extrasynaptic GABA_A receptor mediates tonic inhibition in thalamic VB neurons. *J. Neurophysiol.* **94**, 4491–4501.
- Jones, E.G., and Pons, T.P. (1998). Thalamic and brainstem contributions to large-scale plasticity of primate somatosensory cortex. *Science* **282**, 1121–1125.
- Kim, S.K., and Nabekura, J. (2011). Rapid synaptic remodeling in the adult somatosensory cortex following peripheral nerve injury and its association with neuropathic pain. *J. Neurosci.* **31**, 5477–5482.
- Kharlamov, E.A., Lepšveridze, E., Meparishvili, M., Solomonia, R.O., Lu, B., Miller, E.R., Kelly, K.M., and Mtchedlishvili, Z. (2011). Alterations of GABA_A and glutamate receptor subunits and heat shock protein in rat hippocampus following traumatic brain injury and in posttraumatic epilepsy. *Epilepsy Res.* **95**, 20–34.
- Kim, S.K., Hayashi, H., Ishikawa, T., Shibata, K., Shigetomi, E., Shinozaki, Y., Inada, H., Roh, S.E., Kim, S.J., Lee, G., et al. (2016). Cortical astrocytes rewire somatosensory cortical circuits for peripheral neuropathic pain. *J. Clin. Invest.* **126**, 1983–1997.
- LeBlanc, B.W., Lii, T.R., Huang, J.J., Chao, Y.C., Bowary, P.M., Cross, B.S., Lee, M.S., Vera-Portocarrero, L.P., and Saab, C.Y. (2016). T-type calcium channel blocker Z944 restores cortical synchrony and thalamocortical connectivity in a rat model of neuropathic pain. *Pain* **157**, 255–263.
- Lenz, F.A., Kwan, H.C., Dostrovsky, J.O., and Tasker, R.R. (1989). Characteristics of the bursting pattern of action potentials that occurs in the thalamus of patients with central pain. *Brain Res.* **496**, 357–360.
- Lenz, F.A., Seike, M., Richardson, R.T., Lin, Y.C., Baker, F.H., Khoja, I., Jaeger, C.J., and Gracely, R.H. (1993). Thermal and pain sensations evoked by microstimulation in the area of human ventrocaudal nucleus. *J. Neurophysiol.* **70**, 200–212.
- Lenz, F.A., Garonzik, I.M., Zirh, T.A., and Dougherty, P.M. (1998). Neuronal activity in the region of the thalamic principal sensory nucleus (ventralis caudalis) in patients with pain following amputations. *Neuroscience* **86**, 1065–1081.
- Liang, J., Cagetti, E., Olsen, R.W., and Spigelman, I. (2004). Altered pharmacology of synaptic and extrasynaptic GABA_A receptors on CA1 hippocampal neurons is consistent with subunit changes in a model of alcohol withdrawal and dependence. *J. Pharmacol. Exp. Ther.* **310**, 1234–1245.
- Lois, C., Hong, E.J., Pease, S., Brown, E.J., and Baltimore, D. (2002). Germline transmission and tissue-specific expression of transgenes delivered by lentiviral vectors. *Science* **295**, 868–872.
- Lorenzetto, E., Caselli, L., Feng, G., Yuan, W., Nerbonne, J.M., Sanes, J.R., and Buffelli, M. (2009). Genetic perturbation of postsynaptic activity regulates synapse elimination in developing cerebellum. *Proc. Natl. Acad. Sci. USA* **106**, 16475–16480.
- Lorenzo, L.E., Godin, A.G., Wang, F., St-Louis, M., Carbonetto, S., Wiseman, P.W., Ribeiro-da-Silva, A., and De Koninck, Y. (2014). Gephyrin clusters are absent from small diameter primary afferent terminals despite the presence of GABA_A receptors. *J. Neurosci.* **34**, 8300–8317.

- Mikuni, T., Uesaka, N., Okuno, H., Hirai, H., Deisseroth, K., Bito, H., and Kano, M. (2013). Arc/Arg3.1 is a postsynaptic mediator of activity-dependent synapse elimination in the developing cerebellum. *Neuron* 78, 1024–1035.
- Miyata, M., and Imoto, K. (2006). Different composition of glutamate receptors in corticothalamic and lemniscal synaptic responses and their roles in the firing responses of ventrobasal thalamic neurons in juvenile mice. *J. Physiol.* 575, 161–174.
- Mòdol, L., Cobianchi, S., and Navarro, X. (2014). Prevention of NKCC1 phosphorylation avoids downregulation of KCC2 in central sensory pathways and reduces neuropathic pain after peripheral nerve injury. *Pain* 155, 1577–1590.
- Moore, K.A., Kohno, T., Karchewski, L.A., Scholz, J., Baba, H., and Woolf, C.J. (2002). Partial peripheral nerve injury promotes a selective loss of GABAergic inhibition in the superficial dorsal horn of the spinal cord. *J. Neurosci.* 22, 6724–6731.
- Mowery, T.M., Walls, S.M., and Garraghty, P.E. (2013). AMPA and GABA_{A,B} receptor subunit expression in the cortex of adult squirrel monkeys during peripheral nerve regeneration. *Brain Res.* 1520, 80–94.
- Niwa, H., Yamamura, K., and Miyazaki, J. (1991). Efficient selection for high-expression transfectants with a novel eukaryotic vector. *Gene* 108, 193–199.
- Nomura, H., Ogawa, A., Tashiro, A., Morimoto, T., Hu, J.W., and Iwata, K. (2002). Induction of Fos protein-like immunoreactivity in the trigeminal spinal nucleus caudalis and upper cervical cord following noxious and non-noxious mechanical stimulation of the whisker pad of the rat with an inferior alveolar nerve transection. *Pain* 95, 225–238.
- Ohara, P.T., and Lieberman, A.R. (1985). The thalamic reticular nucleus of the adult rat: experimental anatomical studies. *J. Neurocytol.* 14, 365–411.
- Peden, D.R., Petitjean, C.M., Herd, M.B., Durakoglugil, M.S., Rosahl, T.W., Wafford, K., Homanics, G.E., Belelli, D., Fritschy, J.M., and Lambert, J.J. (2008). Developmental maturation of synaptic and extrasynaptic GABA_A receptors in mouse thalamic ventrobasal neurones. *J. Physiol.* 586, 965–987.
- Peng, Z., Huang, C.S., Stell, B.M., Mody, I., and Houser, C.R. (2004). Altered expression of the δ subunit of the GABA_A receptor in a mouse model of temporal lobe epilepsy. *J. Neurosci.* 24, 8629–8639.
- Radhakrishnan, V., Tsoukatos, J., Davis, K.D., Tasker, R.R., Lozano, A.M., and Dostrovsky, J.O. (1999). A comparison of the burst activity of lateral thalamic neurons in chronic pain and non-pain patients. *Pain* 80, 567–575.
- Ralston, H.J., 3rd, and Ralston, D.D. (1994). Medial lemniscal and spinal projections to the macaque thalamus: an electron microscopic study of differing GABAergic circuitry serving thalamic somatosensory mechanisms. *J. Neurosci.* 14, 2485–2502.
- Rausell, E., Cusick, C.G., Taub, E., and Jones, E.G. (1992). Chronic deafferentation in monkeys differentially affects nociceptive and nonnociceptive pathways distinguished by specific calcium-binding proteins and down-regulates γ -aminobutyric acid type A receptors at thalamic levels. *Proc. Natl. Acad. Sci. USA* 89, 2571–2575.
- Ray, N.J., Jenkinson, N., Kringlebach, M.L., Hansen, P.C., Pereira, E.A., Brittain, J.S., Holland, P., Holliday, I.E., Owen, S., Stein, J., and Aziz, T. (2009). Abnormal thalamocortical dynamics may be altered by deep brain stimulation: using magnetoencephalography to study phantom limb pain. *J. Clin. Neurosci.* 16, 32–36.
- Sametsky, E.A., Turner, J.G., Larsen, D., Ling, L., and Caspary, D.M. (2015). Enhanced GABA_A-mediated tonic inhibition in auditory thalamus of rats with behavioral evidence of tinnitus. *J. Neurosci.* 35, 9369–9380.
- Sano, H., Chiken, S., Hikida, T., Kobayashi, K., and Nambu, A. (2013). Signals through the striatopallidal indirect pathway stop movements by phasic excitation in the substantia nigra. *J. Neurosci.* 33, 7583–7594.
- Seino, H., Seo, K., Maeda, T., and Someya, G. (2009). Behavioural and histological observations of sensory impairment caused by tight ligation of the trigeminal nerve in mice. *J. Neurosci. Methods* 181, 67–72.
- Sherman, S.M. (2001). Tonic and burst firing: dual modes of thalamocortical relay. *Trends Neurosci.* 24, 122–126.
- Steriade, M. (2005). Sleep, epilepsy and thalamic reticular inhibitory neurons. *Trends Neurosci.* 28, 317–324.
- Takeuchi, Y., Yamasaki, M., Nagumo, Y., Imoto, K., Watanabe, M., and Miyata, M. (2012). Rewiring of afferent fibers in the somatosensory thalamus of mice caused by peripheral sensory nerve transection. *J. Neurosci.* 32, 6917–6930.
- Takeuchi, Y., Asano, H., Katayama, Y., Muragaki, Y., Imoto, K., and Miyata, M. (2014). Large-scale somatotopic refinement via functional synapse elimination in the sensory thalamus of developing mice. *J. Neurosci.* 34, 1258–1270.
- Takeuchi, Y., Osaki, H., Yagasaki, Y., Katayama, Y., and Miyata, M. (2017). Afferent fiber remodeling in the somatosensory thalamus of mice as a neural basis of somatotopic reorganization in the brain and ectopic mechanical hypersensitivity after peripheral sensory nerve injury. *eNeuro* 4, e0345–16.
- Tal, M., and Bennett, G.J. (1994). Extra-territorial pain in rats with a peripheral mononeuropathy: mechano-hyperalgesia and mechano-allodynia in the territory of an uninjured nerve. *Pain* 57, 375–382.
- Tsuboi, Y., Takeda, M., Tanimoto, T., Ikeda, M., Matsumoto, S., Kitagawa, J., Teramoto, K., Simizu, K., Yamazaki, Y., Shima, A., et al. (2004). Alteration of the second branch of the trigeminal nerve activity following inferior alveolar nerve transection in rats. *Pain* 111, 323–334.
- Uesaka, N., Uchigashima, M., Mikuni, T., Nakazawa, T., Nakao, H., Hirai, H., Aiba, A., Watanabe, M., and Kano, M. (2014). Retrograde semaphorin signaling regulates synapse elimination in the developing mouse brain. *Science* 344, 1020–1023.
- Vassias, I., Lecolle, S., Vidal, P.P., and de Waele, C. (2005). Modulation of GABA receptor subunits in rat facial motoneurons after axotomy. *Brain Res. Mol. Brain Res.* 135, 260–275.
- Wang, G., and Thompson, S.M. (2008). Maladaptive homeostatic plasticity in a rodent model of central pain syndrome: thalamic hyperexcitability after spinothalamic tract lesions. *J. Neurosci.* 28, 11959–11969.
- Welker, E., Soriano, E., and Van der Loos, H. (1989). Plasticity in the barrel cortex of the adult mouse: effects of peripheral deprivation on GAD-immunoreactivity. *Exp. Brain Res.* 74, 441–452.
- Weng, H.R., Lee, J.I., Lenz, F.A., Schwartz, A., Vierck, C., Rowland, L., and Dougherty, P.M. (2000). Functional plasticity in primate somatosensory thalamus following chronic lesion of the ventral lateral spinal cord. *Neuroscience* 101, 393–401.
- Whissell, P.D., Lecker, I., Wang, D.S., Yu, J., and Orser, B.A. (2015). Altered expression of δ GABA_A receptors in health and disease. *Neuropharmacology* 88, 24–35.
- Wu, X., Huang, L., Wu, Z., Zhang, C., Jiang, D., Bai, Y., Wang, Y., and Chen, G. (2013). Homeostatic competition between phasic and tonic inhibition. *J. Biol. Chem.* 288, 25053–25065.
- Zhang, N., Wei, W., Mody, I., and Houser, C.R. (2007). Altered localization of GABA_A receptor subunits on dentate granule cell dendrites influences tonic and phasic inhibition in a mouse model of epilepsy. *J. Neurosci.* 27, 7520–7531.

STAR★METHODS

KEY RESOURCES TABLE

REAGENT or RESOURCE	SOURCE	IDENTIFIER
Antibodies		
Rabbit anti- α 4 subunit	Phosphosolutions	Cat# 844-GA4N; RRID: AB_2492104
Guinea pig anti- α 1 subunit	Synaptic Systems	Cat# 224 205; RRID: AB_2619929
Rat anti-GFP	Nacalai Tesque	Cat# 04404-84; RRID: AB_10013361
Alexa Fluor-594 anti-rabbit IgG	Thermo Fisher Scintific	Cat# A21207; RRID: AB_141637
Alexa Fluor-488 anti-guinea pig IgG	Jackson ImmunoResearch	Cat# 706-545-148; RRID: AB_2340472
Chemicals, Peptides, and Recombinant proteins		
THIP	Sigma-Aldrich	Cat# T101; CAS# 85118-33-8
Strychnine	Sigma-Aldrich	Cat# 134929; CAS# 57-24-9
D-APV	Tocris	Cat# 0106; CAS# 79055-68-8
NBQX	Tocris	Cat# 0373; CAS# 118876-58-7
Bicuculline methochloride	Tocris	Cat# 0131; CAS# 53552-05-9
CGP55845	Tocris	Cat# 1248; CAS# 149184-22-5
GABA	Nacalai Tesque	Cat# 02006-64; CAS# 56-12-2
Biocytin	Sigma-Aldrich	Cat# B4261; CAS# 576-19-2
Texas Red-conjugated streptavidin	Vector laboratories	Cat# SA-5006; RRID: AB_2336754
Alexa Fluor 633-conjugated streptavidin	Thermo Fisher Scintific	Cat# S21375; RRID: AB_2313500
VECTATAIN Elite ABC Standard Kit	Vector laboratories	Cat# PK-6100; RRID: AB_2336819
DAB (3,3'-diaminobenzidine tetrahydrochloride)	Dojindo	Cat# D006; CAS# 7411-49-6
Fluoromount-G	SouthernBiotech	Cat# 0100-01
ProLong Gold antifade reagent with DAPI	Thermo Fisher Scintific	Cat# P36931
Experimental Models: Organisms/Strains		
Mouse: C57BL/6N	Sankyo Labo Service Corporation	http://www.sankylabo.co.jp/
Mouse: α 4-floxed (B6.129 Gabra4 < tm1.2 Geh > /J)	The Jackson Laboratory	Stock# 006874; RRID:IMSR_JAX:006874
Mouse: Krox20-Cre (STOCK Egr2 < tm2(cre)Pch > /J)	The Jackson Laboratory	Stock# 025744; RRID:IMSR_JAX:025744
Mouse: Ai14 (B6.Cg-Gt(ROSA)26Sor < tm14(CAG-tdTomato)Hze > /J)	The Jackson Laboratory	Stock# 007914 RRID:IMSR_JAX:007914
Oligonucleotides		
"iCre producing primer, forward: CCTGCATGCTCCGCCGGACTCAGATCTC"	This paper/Custom	No account
"iCre producing primer, reverse: CGGTATCGATTCAAGTCCCCATCCTCGAGCA"	This paper/Custom	No account
Recombinant DNA		
FUGW plasmid	Addgene	Cat# 14883 by Dr David Baltimore
psPAX2	Addgene	Cat# 15246
pCAG-VSVG	–	Gift from Dr Arthur Nienhuis
Software and Algorithms		
MATLAB	MathWorks	RRID: SCR_001622
Igor Pro 6	WaveMetrics	RRID: SCR_000325
Mini Analysis Program	Synaptosoft	RRID: SCR_002184
Patch Master	HEKA	N/A
ImageJ	NIH	RRID: SCR_003070
StatView 5.0	SAS	N/A
GraphPad Prism 6	GraphPad Software	RRID: SCR_002798

(Continued on next page)

Continued

REAGENT or RESOURCE	SOURCE	IDENTIFIER
Other		
Slow-release osmotic mini-pump	Durect Corporation	Cat# Alzet model 1700D
Guide cannula	Durect Corporation	Cat# Alzet Brain Infusion Kit 2

RESOURCE AVAILABILITY**Lead Contact**

Further information and requests for resources and reagents should be directed to and will be fulfilled by the Lead Contact, Prof. Mariko Miyata (mmiyata@tamu.ac.jp).

Materials availability

This study did not generate any unique reagents.

Data and code availability

This study did not generate any unique datasets or code.

EXPERIMENTAL MODEL AND SUBJECT DETAILS**Animals**

The present study was conducted in accordance with the Guiding Principles for the Care and Use of Laboratory Animals recommended by Tokyo Women's Medical University. Every effort was made to minimize the number and suffering of animals used in this study. The following mice were used: both sexes of C57BL/6N mice (P14–33; Sankyo Labo Service Corporation, Tokyo, Japan); B6.129 Gabra4 < tm1.2 Geh > /J mice (P14–43; GABA_AR α 4 subunit-floxed mice, referred to herein as α 4-floxed mice; Jackson Laboratory, Bar Harbor, ME, USA) ([Chandra et al., 2006](#)); and Krox20-Ai14 transgenic mice (P21–31) ([Takeuchi et al., 2014](#)). To obtain α 4-floxed homozygotes, male and female α 4-floxed heterozygotes were crossed. Krox20-Ai14 transgenic mice, in which the lemniscal fibers associated with the maxillary principal trigeminal nucleus (PrV2) are labeled with tdTomato, were used to precisely locate recording sites in the VPM associated with the maxillary trigeminal nerve branch (V2) for *in vivo* recording ([Takeuchi et al., 2014](#)). The animals were housed in a room maintained at $23 \pm 1^\circ\text{C}$ with a 12 h light/dark cycle (lights on, 9:00 A.M.). Food and water were available *ad libitum*.

Complete transection of ION

Mice aged P21 were deeply anesthetized by intraperitoneal administration of ketamine (80 mg/kg) and xylazine (10 mg/kg). The ION on the left side of the face was exposed under a dissecting microscope and completely transected using sterilized fine scissors, and the cut planes were separated by a distance of at least 1.0 mm to prevent regeneration. In the sham operation, the ION was exposed without cutting. The skin was then sutured with silk thread. Physiological saline (0.2 mL per animal) was injected subcutaneously to prevent dehydration after the surgery.

METHOD DETAILS**Slice preparation**

The mice were rapidly decapitated under deep isoflurane anesthesia (Abbott Japan, Osaka, Japan), and the brain was cooled in an ice-cold sucrose solution containing (in mM) 234 sucrose, 2.5 KCl, 10 MgCl₂, 0.5 CaCl₂, 1.25 NaH₂PO₄, 25 NaHCO₃, 10 glucose, and 0.5 *myo*-inositol. Horizontal or parasagittal slices (300 μm thickness) were cut with a vibratome (VT1200S; Leica, Nussloch, Germany), transferred into a submerging chamber, and incubated for 30 min with artificial cerebrospinal fluid (ACSF) containing (in mM) 125 NaCl, 2.5 KCl, 1.25 NaH₂PO₄, 1 MgSO₄, 2 CaCl₂, 26 NaHCO₃, and 20 glucose, which was bubbled continuously with a mixture of 95% O₂ and 5% CO₂ at 32°C. Horizontal slices were used for recordings of evoked IPSCs (eIPSCs) in response to minimal stimulation of the RTN ([Cope et al., 2005](#); [Huntsman and Huguenard, 2000](#)). Parasagittal slices were used for recordings of evoked AMPAR-mediated lemniscal EPSCs (eEPSCs), spontaneous IPSCs (sIPSCs), and extrasynaptic GABA_AR currents ([Arsenault and Zhang, 2006](#); [Miyata and Imoto, 2006](#); [Takeuchi et al., 2012](#)).

***In vitro* whole-cell recordings**

Whole-cell voltage-clamp recordings were made from VPM neurons under an upright microscope (BX50WI; Olympus, Tokyo, Japan) with an infrared differential interference contrast video system (C2400-79H; Hamamatsu Photonics, Hamamatsu, Japan). For

recordings of eEPSCs, sEPSCs, and sIPSCs, glass patch pipettes were filled with an internal solution composed of (in mM): 135 Cs methanesulfonate, 10 HEPES, 1 EGTA, 2 MgCl₂, 0.1 CaCl₂, 1 NaCl, 5 QX-314 chloride, 2 ATP-Na₂, 0.5 GTP-Na, and 0.5% biocytin, adjusted to pH 7.3 with CsOH. The osmolality was 290–300 mOsm, the liquid junction potential was +14.7 mV, and the resistance of the patch pipette was 2.5–3.5 MΩ. For recordings of membrane potential (current-clamp), glass patch pipettes were filled with an internal solution composed of (in mM): 150 K-gluconate, 0.5 EGTA, 10 HEPES, 4 MgCl₂, 0.1 CaCl₂, 4 ATP-Na, 0.4 GTP-Na, and 0.5% biocytin, adjusted to pH 7.3 with KOH. The osmolality was 300–305 mOsm, the liquid junction potential was uncompensated. For recordings of eIPSCs, an external solution (in mM: 126 NaCl, 2.95 KCl, 1.25 Na₂PO₄, 2 MgCl₂, 2 CaCl₂, 26 NaHCO₃, and 10 glucose) containing NBQX (20 μM), D-APV (50 μM), and strychnine (1 μM) (Peden et al., 2008), and an internal solution (in mM: 140 CsCl, 1 CaCl₂, 5 QX-314 chloride, 10 HEPES, 10 EGTA, 2 ATP-Mg, and 0.5% biocytin, adjusted to pH 7.3 with CsOH; 300–305 mOsm; liquid junction potential, +13.0 mV) (Peden et al., 2008) were used. For recordings of evoked miniature IPSCs (mIPSCs), after recording a unitary eIPSC, Ca²⁺ in the external solution was replaced with Sr²⁺ (SrCl₂, 4 mM) (Takeuchi et al., 2012). All experiments were performed at 30–32°C. The liquid junction potential was compensated. Series resistances (typically less than 20 MΩ) were monitored online and compensated 70%. Recorded signals were amplified by an EPC10 patch-clamp amplifier (HEKA, Lambrecht, Germany), filtered at 2.9 kHz, and digitized at 20 kHz.

Both the unitary eIPSCs and evoked mIPSCs were elicited at a holding potential of –60 mV with the same stimulus delivered by a concentric electrode (tip diameter, 25 μm; Inter Medical, Nagoya, Japan) placed in the reticular thalamic nucleus (Huntsman and Hu-guenard, 2000). The stimulus consisted of a 200 μs pulse generated by an isolator (BAK Electronics, Oxford, UK) and was delivered at 0.1 Hz. For recording endogenous or agonist-induced extrasynaptic GABA_{AR} currents, bicuculline methochloride (100 μM) or THIP (10 μM) was bath-applied for 5 min or 30 s, respectively, at a holding potential of 0 mV. eEPSCs were elicited by a concentric electrode placed onto the fiber bundle of the medial lemniscus, as reported previously (Arsenault and Zhang, 2006; Miyata and Imoto, 2006; Takeuchi et al., 2012), at a holding potential of –60 or –70 mV. We investigated lemniscal EPSC steps using increments of stimulus intensity to evaluate the lemniscal fiber innervation pattern. Because lemniscal fiber remodeling starts from POD5 (Takeuchi et al., 2012), we recorded neurons on POD6–9, first recording eEPSCs at a holding potential of –60 mV and then recording extrasynaptic GABA_{AR} currents at a holding potential of 0 mV in the same neuron.

To record spontaneous synaptic events, neurons were held at –60 mV (i.e., the reversal potential of IPSCs) for sEPSCs or at 0 mV (i.e., the reversal potential for EPSCs) for sIPSCs. To estimate the balance of excitatory and inhibitory synaptic inputs, we first recorded sEPSCs and sIPSCs, and then recorded extrasynaptic GABA_{AR} currents from the same VPM neurons. We then calculated the excitatory and phasic/tonic inhibitory charges from the recorded synaptic currents. The total number of events in sham neurons, IONC-multiple neurons, and IONC-single neurons was 12168 events (from seven neurons), 12504 events (from eight neurons), and 12936 events (eight neurons), respectively.

The eIPSCs and eEPSCs were acquired and analyzed using a custom-built Igor Pro procedure (tUtility: <https://github.com/yuichi-takeuchi/tUtility>). The mIPSCs, sIPSCs, and sEPSCs were analyzed using the Mini Analysis Program (Synaptosoft Inc., Decatur, GA, USA) or a custom-built Igor Pro procedure (miniAna: <https://github.com/yuichi-takeuchi/miniAna>). The analysis window was 100–500 ms after each stimulus.

Immunohistochemical staining of α subunits of the GABA_{AR}

C57BL/6N mice aged P24 (POD3 after IONC or age-matched normal C57BL/6N mice) were deeply anesthetized with sodium pentobarbital (60–100 mg/kg, intraperitoneally) and perfused transcardially with phosphate-buffered saline (PBS) followed by a fixative (4% paraformaldehyde and 0.2% picric acid in 0.1 M PBS), and postfixed for less than 30 min. The brains were coronally cut into 30 μm sections using a vibratome. Sections were incubated for 24–48 h at 4°C with a rabbit polyclonal antibody against the α4 subunit (844-GA4N; Phosphosolutions, Aurora, CO, USA; 1:300) and a guinea pig polyclonal antibody against the α1 subunit (224 205; Synaptic Systems, Göttingen, Germany; 1:500) in 0.05 M PBS containing 10% normal donkey serum without Triton X-100. After washing in PBS, the sections were reacted with secondary antibodies conjugated to Alexa Fluor 594 (for α4; Thermo Fisher Scientific, Waltham, MA, USA; 1:500) and Alexa Fluor 488 (for α1; Jackson ImmunoResearch, West Grove, PA, USA; 1:500) for 2–3 h at room temperature. The sections were mounted on glass slides and coverslipped with Prolong Gold antifade reagent with DAPI (Thermo Fisher Scientific). Images were acquired using an oil-immersion objective (63 ×) with a resolution of 2048 × 2048 pixels (134.95 × 134.95 μm, z step = 0.5 μm, from the surface to a depth of 3–5 μm) with an LSM 710 confocal laser scanning microscope (Carl Zeiss, Oberkochen, Germany). Two regions of interest were placed in the dorsal part of the VPM in each hemisphere of one section (three sections per animal). Binary masks of clustered staining of α subunits (Lorenzo et al., 2014) were extracted from Zeiss LSM image files using a custom-built software written with MATLAB (MathWorks Inc., Natick, MA, USA).

After the electrophysiological recordings, to confirm lentivirally expressed iCre-GFP, biocytin-filled VPM neurons were fixed with the fixative solution overnight at 4°C and visualized using a Texas Red-conjugated streptavidin (SA-5006; Vector Laboratories, Burlingame, CA, USA) or standard ABC-DAB reaction protocol with cytochrome oxidase counterstain (Takeuchi et al., 2012). To examine α4 subunit expression in recorded neurons, 300 μm-thick sections were re-sectioned at 50 μm. Sections were incubated overnight at 4°C with a rat monoclonal antibody against GFP (04404-84; Nacalai Tesque, Kyoto, Japan; 1:3,000) and a rabbit polyclonal antibody against the α4 subunit in 0.05 M PBS containing 10% normal donkey serum with 0.3% Triton X-100. The sections were further reacted with Alexa Fluor 633-conjugated streptavidin (S21375; Thermo Fisher Scientific; 1:500), and secondary antibodies conjugated to Alexa Fluor 594 (for α4; Thermo Fisher Scientific; 1:500) and Alexa Fluor 488 (for iCre-GFP; Thermo Fisher Scientific; 1:500).

Chronic administration of an extrasynaptic GABA_AR agonist through an osmotic mini-pump

An extrasynaptic GABA_AR agonist, THIP, was chronically applied to the VPM through a slow-release Alzet osmotic mini-pump (1.0 µL/h for 1 week; Alzet model 1700D; Durect Corporation, Cupertino, CA, USA). C57BL/6N mice aged P21 were deeply anesthetized with ketamine (80 mg/kg) and xylazine (10 mg/kg), and placed in a stereotaxic apparatus. The skull was exposed, and a small hole was made using a dental drill. A guide cannula (Alzet Brain Infusion Kit 2; Durect Corporation) was implanted into the right VPM (coordinates in mm: 1.6 posterior and 1.4 lateral to bregma, 3.2 below the dura), according to the mouse brain atlas (Franklin and Paxinos, 2007). The guide cannula was fixed to the skull with cranioplastic cement. A guide cannula was attached to extension tubes and linked to the osmotic mini-pump, which was installed in a subcutaneous pocket on the lateral back of the mouse. After the installation of the osmotic mini-pump, back wounds from the operation were closed with sutures, and the mice were intraperitoneally injected with a solution of 5% glucose (0.3 mL per mouse) to prevent dehydration and supply energy. The osmotic mini-pump was used to directly inject THIP (100 µM) with 0.1% Fast Green into the VPM through a guide cannula chronically for 6–12 days.

Virus preparation and infection

The VSV-G pseudotyped lentiviral vectors were provided by Dr. David Baltimore (through Addgene, FUGW plasmid #14883) (Lois et al., 2002). The vectors were designed to express either GFP or GFP and iCre under the control of the human polyubiquitin-C promoter. Full-length cDNA of iCre was produced by PCR with primers (5'-CCTGCATGCTCCGGCCGGACTCAGATCTC-3' and 5'-CGGTATCGATTCTCAGTCCCCATCCTCGAGCA-3'), linked in-frame, interposed with GFP by a picornavirus “self-cleaving” P2A peptide sequence to enable efficient bicistronic expression, and then subcloned into the *Bam*H1 and *Eco*R1 sites of the FUGW vector. The viral vector was produced by cotransfection of human embryonic kidney 293T cells (2–6 × 10⁶/dish) with a mixture of two packaging plasmids (7 µg psPAX2, Addgene, plasmid 15246; 3 µg pcAG-VSVG, gift from Dr. Arthur Nienhuis) (Niwa et al., 1991), and 10 µg FUGW vector plasmid using a calcium phosphate precipitation method as reported previously (Uesaka et al., 2014).

The GABA_AR α 4 subunit-floxed mice (referred to hereafter as α 4-floxed mice) were anesthetized on P14 or P26 using 3.0%–3.5% isoflurane and placed in a stereotaxic frame. A small volume (400 nL) of lentivirus vector solution was injected into the right VPM (coordinates in mm: 1.35–1.40 posterior and 1.40–1.45 lateral to bregma, 3.20–3.30 below the dura, depending on the weight of the mouse) through a microneedle syringe (NF35BV and NANOFIL; World Precision Instruments, Sarasota, FL, USA) by continuous pressure from a microsyringe pump (Quintessential Stereotaxic Injector 53311; Stoelting Co., Wood Dale, IL, USA). The skin was sutured with silk thread after the infusion of the lentivirus vector and then mice were subcutaneously injected with physiological saline (0.2–0.3 mL per mouse) to prevent dehydration. After 1 week of survival, mice received IONC under deep anesthesia induced with ketamine and xylazine.

In vivo extracellular recording of thalamic neuronal firing in unanesthetized mice

Krox20-Ai14 transgenic mice, in which the lemniscal fibers associated with the maxillary nerve are labeled with tdTomato, were used to locate the exact recording sites (Takeuchi et al., 2014). A custom-made head holder was mounted on the skull, as previously described (Chiken et al., 2008; Sano et al., 2013). Briefly, each mouse was anesthetized with ketamine/xylazine and mounted on a stereotaxic apparatus. The skull was exposed, and the head holder was mounted and fixed with bone-adhesive resin and acrylic resin. Electrodes for recording the electromyogram (EMG) (Chiken et al., 2008) and electrocorticogram (ECoG) were implanted in the triceps brachii muscles and in the parietal cortex to monitor muscle activity and brain electrical activity, respectively. Finally, a craniotomy was performed above the VPM. After surgery, mice were exposed to the recording environment daily for acclimation.

On POD9–10, a mouse was mounted in the stereotaxic apparatus with head fixation without anesthesia. Multi-unit activity in the VPM was recorded via a microelectrode (9–12 MΩ at 1 kHz; FHC, Inc., Bowdoin, ME, USA). The target area was 1.5–1.7 mm posterior and 1.8–1.9 mm lateral from bregma, and 3.0–3.4 mm below the pia. Signals in the VPM were processed with an extracellular amplifier (2400A; Dagan, Minneapolis, MN, USA) and filtered at 250–3000 Hz. The EMG and ECoG signals were filtered at 15–3000 Hz and 0.08–3000 Hz, respectively. Signals were recorded using a 1401 plus interface (Cambridge Electronic Design, Cambridge, UK) with a sampling rate of 50 kHz for multi-unit activity and 6250 Hz for EMG and ECoG signals. After the recordings, several recording sites were electrolytically lesioned (anodal currents; typically 5 µA, 10 s). The mice were then deeply anesthetized, transcardially perfused, and fixed. After removal, the brains were coronally sectioned (50 µm thickness), counterstained with fluoro-Nissl staining, and cover-slipped. Images were acquired using a confocal laser-scanning microscope (Carl Zeiss).

Only VPM recordings associated with the maxillary nerve were analyzed. Data collected during body movements with intense EMG signals were discarded. We analyzed the data with a custom-built Igor Pro procedure (tSort: <https://github.com/yuchi-takeuchi/tSort>). Spikes were sorted by a semi-automated procedure using principal component analysis and clustering followed by manual correction using window discrimination (Figure S6). Each spike was automatically identified as a burst or tonic (non-burst) event (Figure S6). Burst spikes were defined as spikes within a burst episode. A burst episode was initiated by an inter-spike interval (ISI) ≤ 6 ms and ended with a spike preceding an ISI > 10 ms. A burst episode must also have been preceded by an ISI > 20 ms (Lenz et al., 1998).

Tactile sensory test

The VPM of P14 α 4-floxed mice was infused with lentivirus vector under deep isoflurane anesthesia, and mice were then randomly divided into sham and IONC groups. For the control, we injected a lentivirus vector expressing only GFP into the VPM of α 4-floxed

(control) mice. After recovering from the lentivirus injection, the mice were habituated to being held in the experimenter's hands and to von Frey filament application to their maxillary (innervated by the V2 nerve branch) and mandibular (innervated by the V3 nerve branch) regions for 5 days prior to IONC or sham surgery (Seino et al., 2009). On P21, mice received IONC or a sham operation as described above. To evaluate the mechanical withdrawal threshold, von Frey filaments with bending forces of approximately equal logarithmic steps (0.02, 0.03, 0.07, 0.16, 0.4, 0.6, 1.0, and 1.4 g force) were applied to the mandibular and maxillary regions in ascending order of force. Each von Frey filament was applied five times. When mice showed a withdrawal response (e.g., scratching, face moving, or vocalization) to a filament more than three times, the bending force of that filament was defined as the withdrawal threshold. If mice did not show any responses to the 1.4 g force filament, the withdrawal threshold was set at 1.5 g (Dixon, 1980). This series of assessments was repeated two or three times, and the average of these assessments was considered the withdrawal threshold for that mouse on that day. The assessments were performed before IONC and during POD4–5. Ectopic mechanical hypersensitivity was assessed by using von Frey filaments to measure the mechanical withdrawal threshold in the mandibular region. After IONC, the mechanical withdrawal threshold in the mandibular region decreases significantly compared with the pre-IONC threshold, and this change is temporally consistent with lemniscal fiber remodeling (Takeuchi et al., 2017). By contrast, mechanical withdrawal thresholds in the maxillary region after IONC reached the force of the cut-off filament because these mice had no sensation in the maxillary region following IONC.

To evaluate the withdrawal thresholds in the maxillary and mandibular regions in mice treated chronically with THIP, normal mice aged P49–51 had a guide cannula (Alzet Brain Infusion Kit 2) implanted into the right VPM (coordinates in mm: 1.6 posterior and 1.4 lateral to bregma, 3.2 below the dura) according to the mouse brain atlas (Franklin and Paxinos, 2007) under deep anesthesia. Normal mice aged P49–51 were used to reduce surgical invasion by an osmotic mini-pump implantation for analyzing behavioral response. The guide cannula was attached to extension tubes and linked to the osmotic mini-pump filled with 100 μ M THIP and 0.1% Fast Green, which was installed in a subcutaneous pocket on the lateral back of the mouse. Withdrawal threshold assessments were performed before the implantation of the osmotic mini-pump and at POD7.

QUANTIFICATION AND STATISTICAL ANALYSIS

Data for whole-cell recordings from VPM neurons were acquired using Patch Master software (version v2x53; HEKA Instruments Inc., Holliston, MA, USA) and analyzed in Igor Pro software (version 6.3; WaveMetrics, Inc., Portland, OR, USA) or Mini Analysis Program (version 6.0.7; Synaptosoft Inc.). Statistical significance was determined by unpaired Student's t test, paired t test, one-way ANOVA followed by Bonferroni test, Kolmogorov–Smirnov test, χ^2 test, or Mann–Whitney U-test in GraphPad Prism software (version 6.05; GraphPad Software Inc., La Jolla, CA, USA) or StatView software (version 5.0; SAS Institute Inc., Cary, NC, USA). For MATLAB k-means clustering of sham and IONC VPM neurons on the basis of endogenous and antagonist-induced extrasynaptic GABA_AR currents, the optimal number of clusters tested ranged from one to three clusters. All data are presented as the mean \pm SEM.

Supplemental Information

**Tonic GABAergic Inhibition Is Essential for Nerve
Injury-Induced Afferent Remodeling in the
Somatosensory Thalamus and Ectopic Sensations**

Yasuyuki Nagumo, Yoshifumi Ueta, Hisako Nakayama, Hironobu Osaki, Yuichi Takeuchi, Naofumi Uesaka, Masanobu Kano, and Mariko Miyata

Supplemental Information

Tonic GABAergic inhibition is essential for nerve injury-induced afferent remodeling in the somatosensory thalamus and associated ectopic sensations

Yasuyuki Nagumo, Yoshifumi Ueta, Hisako Nakayama, Hironobu Osaki, Yuichi Takeuchi, Naofumi Uesaka, Masanobu Kano, and Mariko Miyata

Contents:

Supplemental Figures

Figure S1: Infraorbital nerve cut (IONC) induces abnormal remodeling of afferent lemniscal fibers in the somatosensory thalamus (related to Figure 1 of the main text).

Figure S2: Two clusters of VPM neurons can be identified on the basis of the amplitude of extrasynaptic GABA_{AR} currents during the early stages of remodeling (related to Figure 1 of the main text).

Figure S3: IONC rapidly reduces synaptic GABA_{AR} currents in VPM neurons (related to Figure 1 of the main text).

Figure S4: THIP affects extrasynaptic, but not synaptic, GABA_{AR} currents in $\alpha 4$ deleted VPM neurons (related to Figure 5 of the main text).

Figure S5: Application of THIP *in vitro* facilitates burst firing of VPM neurons (related to Figure 1-6 of the main text).

Figure S6: IONC increases burst mode *in vivo* (related to Figure 1-6 of the main text).

Figure S7: Effect of conditional deletion or pharmacological enhancement of extrasynaptic GABA_{AR} currents on mechanical withdrawal thresholds in the mandibular and maxillary regions (related to Figure 7 of the main text).

Supplemental Tables

Table S1: Agonist-induced and endogenous extrasynaptic GABA_AR currents in VPM neurons (related to Figure 1 of the main text).

Table S2: IONC-induced changes in immunoreactivity of GABA_AR $\alpha 4$ and $\alpha 1$ subunits in the VPM (related to Figure 2 of the main text).

Table S3: Inhibitory and excitatory input intensities on VPM neurons (related to Figure 3 of the main text).

Table S4: Single fiber and the maximum EPSC amplitudes in VPM neurons (related to Figures 4–6 of the main text).

Table S5: Withdrawal thresholds for mechanical stimulation to the mandibular or maxillary region using von Frey filaments in IONC-operated mice (related to Figure 7 of the main text).

Figure S1

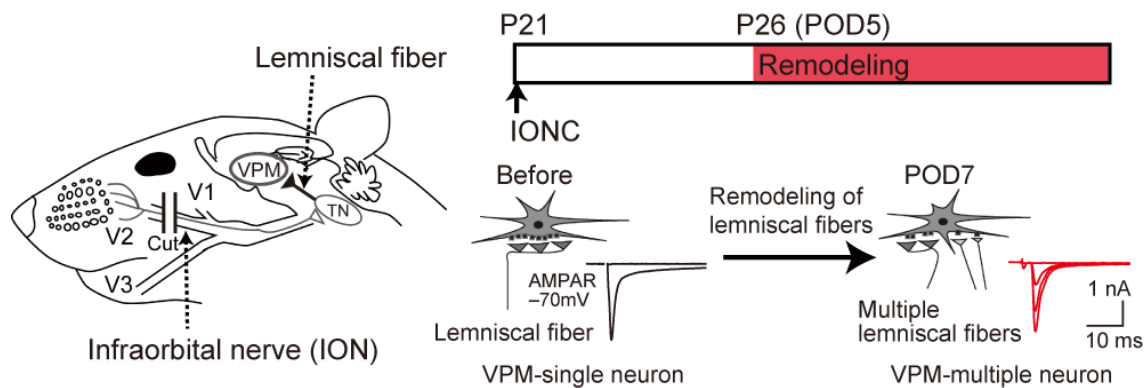


Figure S1: Infraorbital nerve cut (IONC) induces abnormal remodeling of afferent lemniscal fibers in the somatosensory thalamus (related to Figure 1 of the main text). Schema showing lemniscal fiber remodeling after IONC. TN, trigeminal nuclei; VPM, thalamic ventral posterior medial nucleus; V1, ophthalmic trigeminal nerve branch; V2, maxillary trigeminal nerve branch; V3, mandibular trigeminal nerve branch; AMPAR, AMPA receptor; POD, postoperative day.

Figure S2

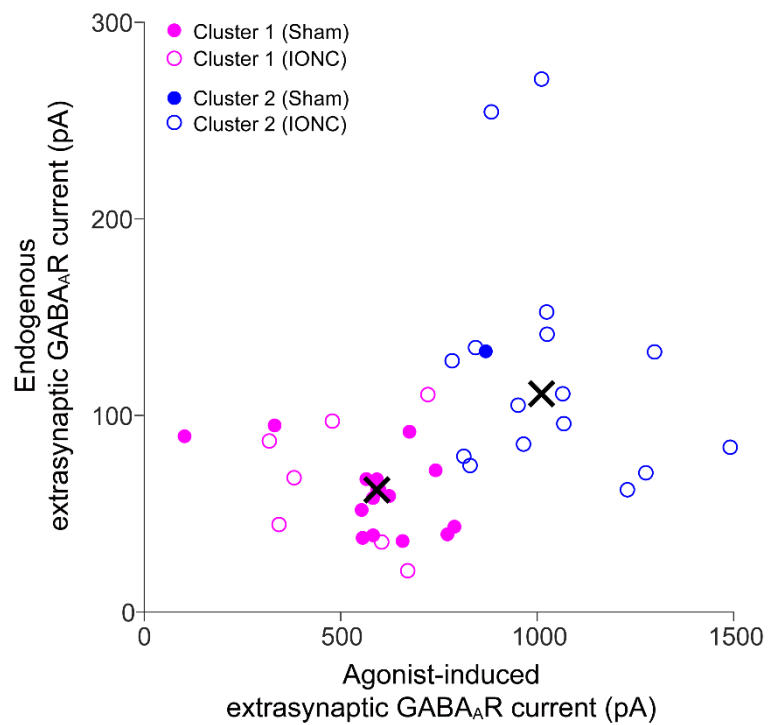


Figure S2: Two clusters of VPM neurons can be identified on the basis of the amplitude of extrasynaptic GABA_AR currents during the early stages of remodeling (related to Figure 1 of the main text).

The cross marks indicate the centroids of each cluster. VPM neurons were obtained from sham and IONC mice during POD1–5. The first cluster (magenta) includes 16 neurons from sham animals (filled circles) and seven neurons from IONC animals (open circles). The second cluster (blue) includes one neuron from a sham animal and 14 neurons from IONC animals.

Figure S3

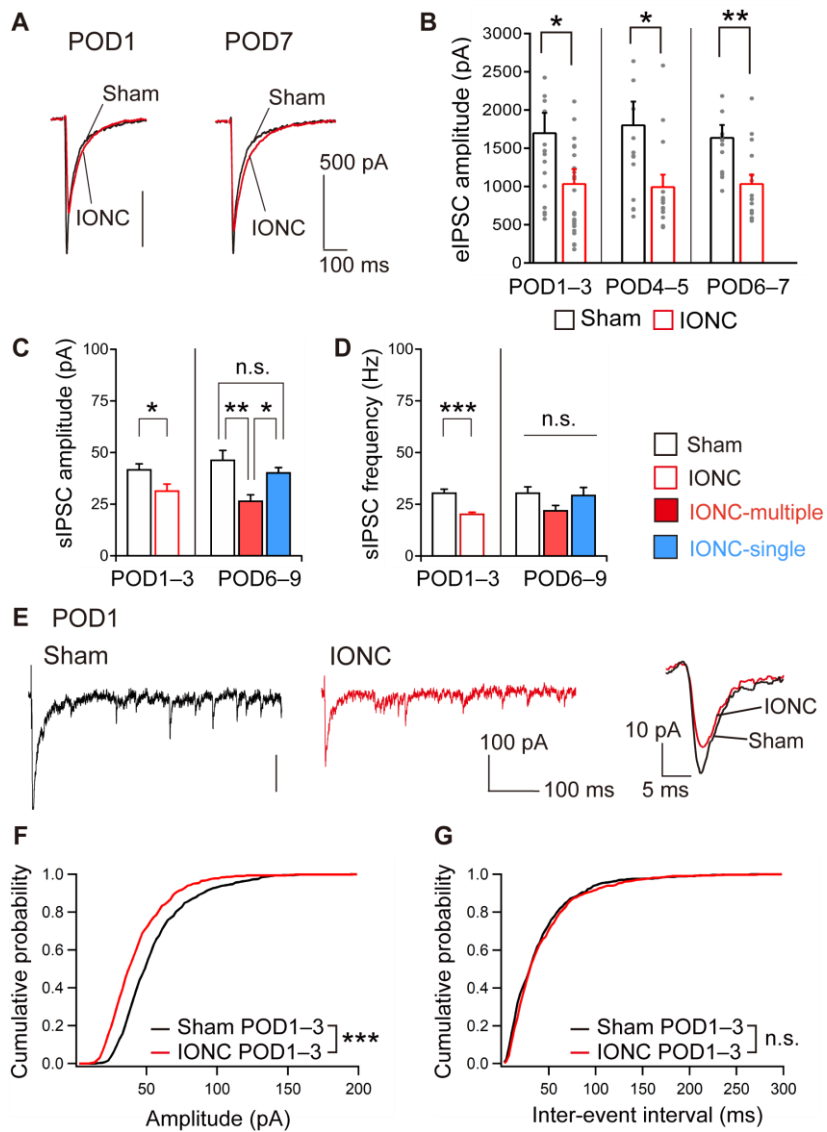


Figure S3: IONC rapidly reduces synaptic GABA_AR currents in VPM neurons (related to Figure 1 of the main text).

(A) Representative traces of evoked IPSCs (eIPSCs) induced in VPM neurons at POD1 and POD7 by minimal stimulation of the reticular thalamic nucleus. Holding potential was -60 mV.

(B) Summary graphs showing the mean eIPSC amplitudes grouped by the number of days after IONC. POD1–3: 1033 ± 193.1 pA for IONC ($n = 26$ neurons) and 1697 ± 264.8 pA for sham ($n = 18$); POD4–5: 993.1 ± 161.1 pA for IONC ($n = 14$) and 1801 ± 311.0 pA for sham ($n = 14$); POD6–9: 1032 ± 124.3 pA for IONC ($n = 26$) and 1636 ± 169.0 pA for sham ($n = 23$). Data represent the mean \pm SEM. * $p < 0.05$; ** $p < 0.01$; unpaired

Student's *t*-test.

(C) Summary bar graph showing the mean amplitudes of spontaneous IPSCs (sIPSCs) recorded during POD1–3 and POD6–9. POD1–3: 31.3 ± 3.4 pA for IONC ($n = 10$ neurons) and 41.6 ± 2.9 pA for sham ($n = 8$); POD6–9: 26.4 ± 2.6 pA for IONC-multiple ($n = 8$), 46.2 ± 4.8 pA for sham ($n = 7$), and 40.1 ± 4.8 pA for IONC-single ($n = 7$). Data represent the mean \pm SEM. * $p < 0.05$; ** $p < 0.01$; unpaired Student's *t*-test or one-way ANOVA followed by post hoc Bonferroni test. n.s., not significant.

(D) Summary bar graph showing the mean frequencies of sIPSCs recorded during POD1–3 and POD6–9. POD1–3: 20.1 ± 1.0 Hz for IONC ($n = 10$ neurons) and 30.3 ± 2.0 Hz for sham ($n = 8$); POD6–9: 21.8 ± 2.6 Hz for IONC-multiple ($n = 8$), 30.3 ± 3.1 Hz for sham ($n = 7$), and 29.2 ± 3.9 Hz for IONC-single ($n = 7$). Data represent the mean \pm SEM. *** $p < 0.001$; unpaired Student's *t*-test. n.s., not significant.

(E) Representative traces of miniature IPSCs (mIPSCs) in a VPM cell, evoked from a reticular thalamic fiber. Ca^{2+} (2 mM) in normal ACSF was replaced with Sr^{2+} (4 mM) to record the mIPSCs. Overlay traces were average traces of mIPSCs in sham neurons and IONC neurons.

(F) Cumulative curves showing the amplitudes of mIPSCs during POD1–3. Data were obtained from 812 events ($n = 8$ neurons) for IONC (43.2 ± 0.9 pA) or 783 events ($n = 8$) for sham (55.2 ± 0.9 pA). *** $p < 0.001$; Kolmogorov–Smirnov test. n.s., not significant.

(G) Cumulative curves showing the inter-event intervals of mIPSCs during POD1–3. IONC: 43.7 ± 1.6 ms; and sham: 40.8 ± 1.5 ms. n.s., not significant.

Figure S4

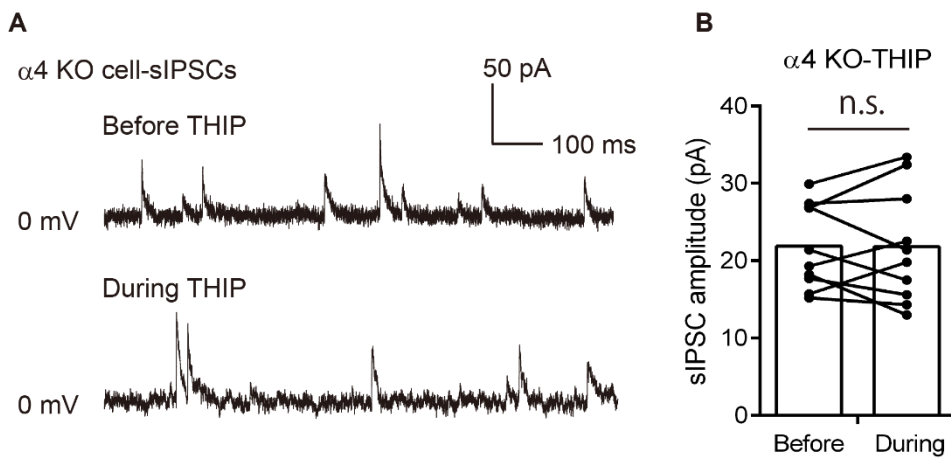


Figure S4: THIP affects extrasynaptic, but not synaptic, GABAAR currents in $\alpha 4$ -deleted VPM neurons (related to Figure 5 of the main text).

(A) Representative sIPSC traces from VPM neurons lacking $\alpha 4$ subunits before (upper) and during (lower) application of THIP ($10 \mu\text{M}$).

(B) Summary plots and bar graphs showing the mean sIPSC amplitude in $\alpha 4$ -deleted VPM neurons before (21.9 pA , $n = 10$ neurons) and during THIP treatment (21.8 pA , $n = 10$ neurons). n.s., not significant, paired Student's *t*-test.

Figure S5

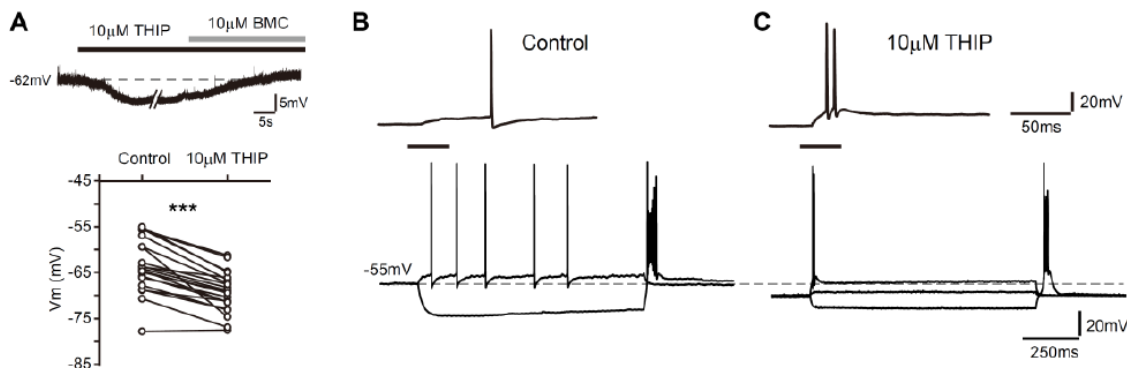


Figure S5: Application of THIP *in vitro* facilitates burst firing of VPM neurons (related to Figures 1–6 of the main text).

(A) Upper: Representative trace of the membrane potential during bath application of 10 μ M THIP and subsequent application of 10 μ M bicuculline methochloride (BMC). Lower: Plots showing the shift in membrane potential for each VPM neuron before (-63.4 ± 5.85 mV, $n = 21$ neurons) and after THIP application (-69.3 ± 4.40 mV, $n = 21$ neurons). $***p < 0.001$, paired Student's t -test.

(B) Specimen traces of the voltage responses to depolarizing and hyperpolarizing current injections of ± 150 pA recorded in a VPM neuron without THIP (control). Depolarizing currents were applied from -55 mV. Inset trace is an enlargement of the initial part of the voltage response.

(C) Voltage responses of the same VPM neuron as shown in (B) during THIP application in response to current injections of -150, +150, and +250 pA. The membrane potential was hyperpolarized to -65 mV.

Figure S6

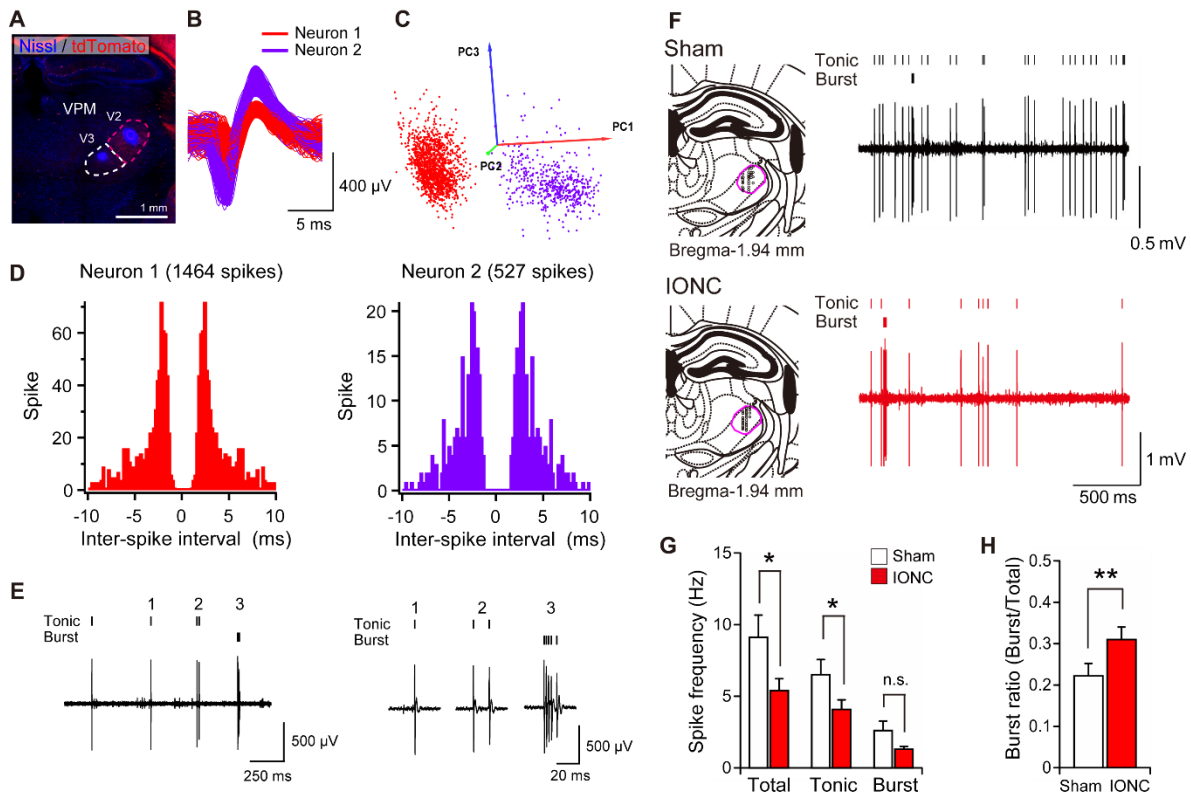


Figure S6: IONC increases burst spike ratio *in vivo* (related to Figures 1–6 of the main text).

- (A) Spikes were only recorded in the VPM associated with V2 innervation of the lemniscus. Dense tdTomato-labeled lemniscal fiber terminals clearly indicate the V2-associated region of the VPM in Krox20-Ai14 mice (magenta-outlined region). Scale bars, 1 mm.
- (B) Representative unit spike waveforms from two distinct neurons in the VPM associated with the whiskers. Spike amplitudes were smaller in neuron 1.
- (C) The first three principal components of the spike waveform can successfully extract two single units. Arrows, contribution vectors. Principal component analysis was conducted on the spike waveforms.
- (D) Auto-correlograms of the units revealed in (B) and (C).
- (E) Left: Representative traces of tonic and burst spikes in the VPM. Right: Time-magnified views of the tonic and burst spikes shown in the left trace. Each event is identified by the number above. Burst episodes were defined as starting with an inter-spike interval (ISI) \leq 6 ms and ending with a spike preceding an ISI $>$ 10 ms.

(F) Representative traces of VPM neuronal firing in magenta-outlined region. Recording sites marked by electrolytic lesions were reconstructed using the brain atlas. Spikes were classified as tonic or burst on the basis of the inter-spike intervals.

(G) Summary graph showing the spike frequencies in sham and IONC neurons. Total spikes: 5.1 ± 0.8 Hz for IONC ($n = 41$ neurons) and 9.1 ± 1.5 Hz for sham ($n = 30$). Tonic spikes: 3.8 ± 0.7 Hz for IONC ($n = 41$) and 6.5 ± 1.1 Hz for sham ($n = 30$). Burst spikes: 1.3 ± 0.2 Hz for IONC ($n = 41$) and 2.6 ± 0.7 Hz for sham ($n = 30$). Data represent the mean \pm SEM. * $p < 0.05$; Mann–Whitney U -test. n.s., not significant.

(H) The proportion of burst spikes to total (tonic and burst) spikes in sham and IONC neurons. Burst ratio: 0.31 ± 0.03 for IONC ($n = 41$) and 0.22 ± 0.03 for sham ($n = 30$). Data represent the mean \pm SEM. ** $p < 0.01$; Mann–Whitney U -test.

Figure S7

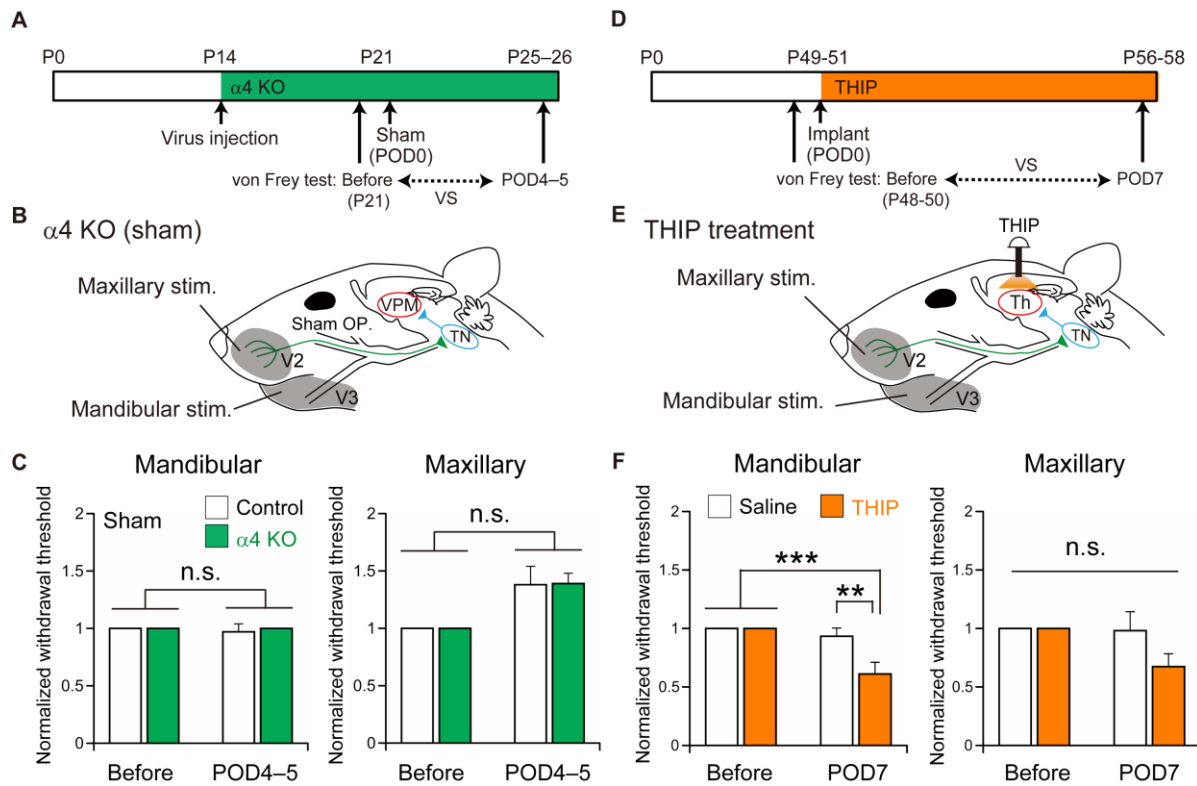


Figure S7: Effect of conditional deletion or pharmacological enhancement of extrasynaptic GABAAR currents on mechanical withdrawal thresholds in the mandibular and maxillary regions (related to Figure 7 of the main text).

(A) Experimental schedule for behavioral tests with lentivirus vector-injected $\alpha 4$ -floxed mice.

(B) Schematic drawing of mechanical stimulation areas in sham-operated mice. OP, operation.

(C) Summary bar graphs showing the changes in mechanical withdrawal thresholds in the mandibular (left) and maxillary (right) regions ipsilateral to the sham operation. Withdrawal thresholds of the test performed before sham operation were normalized as 1 in each animal. At POD4–5, withdrawal thresholds for both mandibular stimulation (0.97 ± 0.03 , 6 mice for control; 1.00 ± 0.0 , 3 mice for $\alpha 4$ KO) and maxillary stimulation (1.38 ± 0.16 for control; 1.39 ± 0.09 for $\alpha 4$ KO) were similar to the baseline level. Data represent the mean \pm SEM. n.s., not significant by post hoc Bonferroni test following one-way ANOVA.

(D) Experimental schedule for behavioral tests with chronic THIP infusion into the somatosensory thalamus of normal mice aged P49–51.

(E) Schematic drawing of mechanical stimulation areas in THIP-treated mice.
(F) Summary bar graphs showing the changes in mechanical withdrawal thresholds in the mandibular (left) and maxillary (right) regions of THIP-treated mice. Withdrawal thresholds of the test performed before THIP treatment were normalized as 1 in each animal. At POD7, THIP treatment tended to lower withdrawal thresholds for both mandibular stimulation (0.93 ± 0.07 , 11 mice for saline-treated; 0.61 ± 0.10 , 12 mice for THIP-treated) and maxillary stimulation (0.98 ± 0.16 for saline-treated and 0.67 ± 0.11 for THIP-treated). Data represent the mean \pm SEM. ** $p < 0.01$; *** $p < 0.001$; one-way ANOVA followed by post hoc Bonferroni test. n.s., not significant.

Table S1: Agonist-induced and endogenous extrasynaptic GABA_AR currents in VPM neurons (related to Figure 1 of the main text).

Agonist-induced (pA)	Sham	IONC	Statistics
POD1–3	543.1 ± 73.6 (12)	930.1 ± 99.8 (12)	Sham < IONC ²
POD4–5	666.6 ± 30.0 (12)	854.0 ± 63.8 (16)	Sham < IONC ¹
	Sham	IONC-single	IONC-multiple
POD6–9	572.7 ± 42.6 (14)	554.0 ± 87.4 (10)	922.6 ± 84.5 (15)
			Sham ³ or IONC-single ³ < IONC-multiple
Endogenous (pA)	Sham	IONC	Statistics
POD1–3	72.3 ± 3.6 (12)	123.2 ± 21.9 (12)	Sham < IONC ¹
POD4–5	61.2 ± 7.5 (13)	106.0 ± 13.6 (16)	Sham < IONC ¹
	Sham	IONC-single	IONC-multiple
POD6–9	90.3 ± 11.1 (14)	73.8 ± 11.3 (11)	176.9 ± 17.2 (15)
			Sham ⁴ or IONC-single ⁴ < IONC-multiple

(n), number of recorded neurons.

¹p < 0.05, ²p < 0.01; unpaired Student's *t*-test.

³p < 0.01, ⁴p < 0.001; one-way ANOVA followed by post hoc Bonferroni test.

Table S2: IONC-induced changes in immunoreactivity of GABA_AR $\alpha 4$ and $\alpha 1$ subunits in the VPM (related to Figure 2 of the main text).

IONC/normal ratio	$\alpha 4$ subunit	$\alpha 1$ subunit	Statistics
Cluster density	5.50 ± 0.18 (3)	1.09 ± 0.18 (3)	$\alpha 4 > \alpha 1^1$
Cluster area	5.99 ± 0.20 (3)	1.08 ± 0.22 (3)	$\alpha 4 > \alpha 1^1$

(n), number of used animals.

¹p < 0.001; unpaired Student's *t*-test.

Table S3: Inhibitory and excitatory input intensities on VPM neurons (related to Figure 3 of the main text).

Charges at POD6–9 (pC)	Sham	IONC-single	IONC-multiple	Statistics
Inhibitory phasic	7.0 ± 0.7 (7)	4.2 ± 0.5 (8)	6.8 ± 0.7 (7)	Sham > IONC-single ¹
Inhibitory tonic	62.4 ± 9.1 (7)	95.1 ± 14.3 (7)	208.7 ± 21.6 (8)	Sham ² or IONC-single ² > IONC-multiple
Inhibitory total	70.4 ± 9.3 (7)	101.8 ± 12.8 (7)	212.3 ± 20.6 (8)	Sham ² or IONC-single ² > IONC-multiple
Excitatory	1.2 ± 0.1 (7)	1.2 ± 0.1 (7)	1.0 ± 0.1 (8)	n.s.

(n), number of recorded neurons.

¹p < 0.05, ²p < 0.001; one-way ANOVA followed by post hoc Bonferroni test.

n.s., not significant.

Table S4: Single fiber and the maximum EPSC amplitudes in VPM neurons (related to Figures 4–6 of the main text).

(related to Fig. 4)	Saline-treated	THIP-treated	Statistics
Single fiber amplitude (nA)	1.98 ± 0.36 (25)	1.23 ± 0.42 (20)	Control > α 4 KO ¹
Maximum amplitude (nA)	2.12 ± 0.35 (25)	1.81 ± 0.46 (20)	n.s.
(related to Fig. 5)	Control	α 4 KO (from P14)	Statistics
Single fiber amplitude (nA)	1.15 ± 0.31 (21)	1.89 ± 0.36 (26)	Control < α 4 KO ¹
Maximum amplitude (nA)	2.36 ± 0.41 (21)	2.24 ± 0.31 (26)	n.s.
(related to Fig. 6)	Control	α 4 KO (from P26)	Statistics
Single fiber amplitude (nA)	1.42 ± 0.25 (28)	1.22 ± 0.23 (17)	n.s.
Maximum amplitude (nA)	2.09 ± 0.23 (28)	1.34 ± 0.21 (17)	Control > α 4 KO ¹

(n), number of recorded neurons.

¹p < 0.05; unpaired Student's *t*-test.

n.s., not significant.

Table S5: Withdrawal thresholds for mechanical stimulation to the mandibular or maxillary region using von Frey filaments in IONC-operated mice (related to Figure 7 of the main text).

Mandibular stimulation (related to Figure 7)	IONC (control)	IONC ($\alpha 4$ KO)	Statistics
Before IONC	1.00 ± 0.0 (12)	1.00 ± 0.0 (10)	Control: before > POD4–5 ¹ $\alpha 4$ KO: before > POD4–5 ¹
POD4–5	0.49 ± 0.04 (12)	0.72 ± 0.06 (10)	POD4–5: control < $\alpha 4$ KO ¹
Maxillary stimulation (related to Figure 7)	IONC (control)	IONC ($\alpha 4$ KO)	Statistics
Before IONC	1.00 ± 0.0 (12)	1.00 ± 0.0 (10)	Control: before > POD4–5 ¹ $\alpha 4$ KO: before > POD4–5 ¹
POD4–5	45.2 ± 2.7 (12)	45.2 ± 2.7 (10)	POD4–5: n.s.

Withdrawal thresholds of the test performed before IONC operation were normalized as 1 in each animal.

(n), number of used animals.

¹p < 0.001; one-way ANOVA followed by post hoc Bonferroni test.

n.s., not significant.